Effects of heterogeneous elasticity coupled to plasticity on stresses and lattice rotations in bicrystals: A Field Dislocation Mechanics viewpoint

Thiebaud Richeton, Stéphane Berbenni

European Journal of Mechanics A/Solids 37 (2013) 231-247
http://dx.doi.org/10.1016/j.euromechsol.2012.06.010

Effects of heterogeneous elasticity coupled to plasticity on stresses and lattice rotations in bicrystals: a Field Dislocation Mechanics viewpoint

T. Richeton[1*], S. Berbenni[1]
[1]*Laboratoire d'Étude des Microstructures et de Mécanique des Matériaux (LEM3), UMR CNRS 7239, Université de Lorraine, Ile du Saulcy, 57045 Metz Cedex 1, France*

Abstract
In the present paper, the static Field Dislocation Mechanics (FDM) theory is first recalled and next formulated for heterogeneous elasticity and plasticity with respect to a reference homogeneous medium. The issue of an infinite bicrystal with planar boundary undergoing piecewise uniform plastic distortions and elastic properties is then considered. The static FDM theory is accordingly used to derive explicit closed-form solutions of stress and lattice misorientation fields in the general context of heterogeneous anisotropic elasticity. These expressions are validated by Crystal Plasticity Finite Element simulations performed on a bicrystal with periodic boundary conditions. As a result of analytical expressions, it is possible to quantify the contribution of the different incompatibility sources, namely the contribution arising from elastic incompatibilities alone, that due to plastic incompatibilities alone and the one due to couplings between elastic and plastic incompatibilities. Besides, residual stresses and lattice misorientations are accordingly calculated in elastic/plastic bicrystals for different orientations of the elastic crystal. Results are compared with the corresponding homogeneous isotropic elasticity approximation. It is shown that elastic-plastic coupling incompatibilities may have consequent effects on residual stresses and lattice misorientations depending on the degree of elastic anisotropy of the material and the relative orientation of both crystals. As a conclusion, the consideration of coupling incompatibilities in multiscale plasticity models when predicting internal stresses and texture developments is discussed.

Keywords: Bicrystals; Incompatibilities; Internal stresses; Lattice rotations; Field Dislocation Mechanics; Jump conditions

1. Introduction

Many studies coupling experiments and theoretical investigations (e.g., Gemperlova et al., 1989; Hirth, 1972; Liang and Dunne, 2009; Mayama et al., 2009; Ohashi et al., 2009; Rey and Zaoui, 1980; 1982; Saada, 2006; Sun et al., 1998; Sutton and Balluffi, 1995; Vehoff et al., 1987; 2004) have been carried out on bicrystals in order to get a better understanding of the specific role of grain boundaries during the deformation of polycrystals. At a material surface of discontinuity (grain, twin or phase boundary), incompatibility stresses can develop due to material elastic anisotropy. Much theoretical work (e.g., Gemperlova et al., 1989; Qamar and Husain,1989; Tewary et al., 1988), including Finite Element simulations (e.g., Schick et al., 2000; Vehoff et al., 2004), has

[*]Corresponding author. Tel.: +33 3 87 31 53 62; Fax: +33 3 87 31 53 66.
E-mail adress: thiebaud.richeton@univ-lorraine.fr

been devoted to estimate these elastic incompatibility stresses in order to predict crack initiation and propagation path. When plasticity enters into play, plastic strain incompatibilities add to the picture and yield additional stresses and lattice rotations. Among these fields, it may actually be distinguished between those uniquely due to a difference in plastic distortions and those arising from a coupling between elastic and plastic heterogeneities. Many models make an assumption of homogeneous isotropic elasticity or of pure rigid viscoplastic behavior (no elasticity) and thus overlook the contribution of both elastic and elastic-plastic coupling incompatibilities. The present paper aims notably at underlying the potentially significant role of coupling incompatibilities. For this purpose, explicit closed-form solutions of stress and lattice misorientation fields are derived for two semi-infinite crystals undergoing uniform plastic distortions in the general context of heterogeneous anisotropic elasticity. The derivation is performed by means of the concepts of the elastic theory of continuously distributed dislocations (ECDD) initiated by Kröner (1958, 1981) and Willis (1967). It deals with the Nye's tensor $\boldsymbol{\alpha}$ (Nye, 1953) which reflects only the so-called geometrically necessary dislocations (GND) densities following Ashby (1970), also referred to as "excess" or "polar" dislocation densities in the literature. The Nye's tensor $\boldsymbol{\alpha}$ is a continuous rendition of the collective arrangements of dislocations and the associated lattice incompatibility. This theory was rethought some years ago by Acharya (2001) (see also Acharya, 2004; Acharya and Roy, 2006) in considering the permanent deformation arising due to dislocation motion. In the Field Dislocation Mechanics (FDM) theory of Acharya (2001), the elastic distortions are uniquely decomposed into compatible and incompatible parts whereas the evolution equation for the GNDs (Mura, 1963) is added within an efficient numerical set-up.

Incompatibility problems constitute a long-standing issue of materials mechanics (see the pioneering works of Bilby, 1955; Frank, 1950; Indenbom 1966; Kröner, 1958; Willis 1967). Different techniques have been envisaged to address these issues and determine stresses and lattice rotations: Green functions (Berveiller and Zaoui, 1980; Berveiller et al., 1987; Kröner, 1989), stress potential functions for plane problems (Kröner, 1981; Berveiller, 1978) or Fourier Transforms (Berbenni et al., 2008; Rey and Saada, 1976; Saada, 1979). In the case of bicrystals, Gemperlova et al. (1989) imagine the total stresses as a sum of the applied and compatibility stresses and the total strains as a sum of elastic strains in relation with applied stresses, elastic strains in relation with compatibility stresses and plastic strains. Then, they consider boundary conditions for stresses and compatibility conditions for strains at the interface to find out the stresses. For three-dimensional heterogeneous elasticity problems, Michelitsch and Wunderlin (1996) have extended the Kröner stress function method. It is also noteworthy that some homogenization schemes for laminates microstructures were derived to calculate the stresses using elastic stress concentration and influence tensors (e.g., Franciosi and Berbenni, 2007, 2008; Stupkiewicz and Petryk, 2002). Netherveless, to the authors' knowledge, no explicit closed-form formulas of stresses have been given for bicrystals with completely anisotropic elasticity and heterogeneous plasticity. In addition, the context of the present paper is different from the preceding approaches since it aims at directly applying the FDM theory (Acharya, 2001) in its static form.

The paper outline is as follows. In Section 2, notation conventions are settled. The static FDM theory is recalled in Section 3 and formulated for heterogeneous elasticity and plasticity with respect to a reference homogeneous medium. Conventional continuity conditions at surfaces of discontinuity are also recalled in this section, in addition to the expression of the surface-dislocation density tensor and the jump condition ensuring the conservation of the Burgers vector. Section 4 deals with the issue of an infinite bicrystal

with planar boundary undergoing piecewise uniform plastic distortions and elastic properties. The static FDM theory is accordingly used to derive analytical expressions of stress and lattice rotation fields in the general case of heterogeneous anisotropic elasticity. The validations of these explicit formulae are checked in Section 5 from Crystal Plasticity Finite Element simulations on a bicrystal with periodic boundary conditions assuming each crystal has a cubic symmetry (fcc metals). The contribution of the different sources of incompatibilities is further analyzed. In Section 5, analytical expressions of residual stresses and lattice misorientations are also used to perform comparisons with results derived from the isotropic approximation. Finally, concluding remarks follow.

2. Notations

A bold symbol denotes a tensor and $\mathbf{v}\otimes\mathbf{w}$ the tensorial product of tensors $\mathbf{v}$ and $\mathbf{w}$. We denote $\mathbf{Av}$ the action of the second-order tensor $\mathbf{A}$ on the vector $\mathbf{v}$, producing a vector. The symbol $\mathbf{AB}$ represents tensor multiplication of the second-order tensors $\mathbf{A}$ and $\mathbf{B}$ and a ":" denotes the contracted product between two tensors. The operation $\times$ is the tensorial cross product, defined as: $\forall\mathbf{c}$, $\left(\mathbf{A}\times\mathbf{v}\right)^{\mathrm{T}}\mathbf{c}=\left(\mathbf{A}^{\mathrm{T}}\mathbf{c}\right)\times\mathbf{v}$, the symbol $\forall$ being shorthand for "for all" and the superscript T denoting the transpose of a matrix. If $\mathbf{A}$ and $\mathbf{B}$ are second-order tensors, $\mathbf{C}$ a fourth-order tensor and $\mathbf{v}$ a vector, we have in rectangular Cartesian coordinates

$$
\begin{aligned}
\left(\mathbf{A}^{\mathrm{T}}\right)_{ij} &= A_{ji}\\
\left(\mathbf{Av}\right)_{i} &= A_{ij}v_{j}\\
\left(\mathbf{AB}\right)_{il} &= A_{ij}B_{jl}\\
\left(\mathbf{C}:\mathbf{A}\right)_{il} &= C_{ilmn}B_{mn}\\
\left(\operatorname{grad}\mathbf{v}\right)_{il} &= v_{i,l}\\
\left(\operatorname{curl}\mathbf{A}\right)_{il} &= \in_{ljk} A_{ik,j}\\
\left(\mathbf{A}\times\mathbf{v}\right)_{il} &= \in_{ljk} A_{ij}v_{k}\\
\left(\mathbf{v}\times\mathbf{w}\right)_{i} &= \in_{ijk} v_{j}w_{k}
\end{aligned}
\qquad (1)
$$

where $\in_{jkl}$ is a component of the third-order alternating Levi-Civita tensor.

Besides, the following reduction convention is adopted concerning the writing of the Hooke's law in matrix notation

$$
(2)\quad
\begin{bmatrix}\sigma_{11}\\ \sigma_{22}\\ \sigma_{33}\\ \sigma_{12}\\ \sigma_{31}\\ \sigma_{23}\end{bmatrix}=
\begin{bmatrix}c_{11}&c_{12}&c_{13}&c_{14}&c_{15}&c_{16}\\ c_{12}&c_{22}&c_{23}&c_{24}&c_{25}&c_{26}\\ c_{13}&c_{23}&c_{33}&c_{34}&c_{35}&c_{36}\\ c_{14}&c_{24}&c_{34}&c_{44}&c_{45}&c_{46}\\ c_{15}&c_{25}&c_{35}&c_{45}&c_{55}&c_{56}\\ c_{16}&c_{26}&c_{36}&c_{46}&c_{56}&c_{66}\end{bmatrix}
\begin{bmatrix}\varepsilon^{e}_{11}\\ \varepsilon^{e}_{22}\\ \varepsilon^{e}_{33}\\ 2\varepsilon^{e}_{12}\\ 2\varepsilon^{e}_{31}\\ 2\varepsilon^{e}_{23}\end{bmatrix}
\quad
\begin{bmatrix}\varepsilon^{e}_{11}\\ \varepsilon^{e}_{22}\\ \varepsilon^{e}_{33}\\ 2\varepsilon^{e}_{12}\\ 2\varepsilon^{e}_{31}\\ 2\varepsilon^{e}_{23}\end{bmatrix}=
\begin{bmatrix}s_{11}&s_{12}&s_{13}&s_{14}&s_{15}&s_{16}\\ s_{12}&s_{22}&s_{23}&s_{24}&s_{25}&s_{26}\\ s_{13}&s_{23}&s_{33}&s_{34}&s_{35}&s_{36}\\ s_{14}&s_{24}&s_{34}&s_{44}&s_{45}&s_{46}\\ s_{15}&s_{25}&s_{35}&s_{45}&s_{55}&s_{56}\\ s_{16}&s_{26}&s_{36}&s_{46}&s_{56}&s_{66}\end{bmatrix}
\begin{bmatrix}\sigma_{11}\\ \sigma_{22}\\ \sigma_{33}\\ \sigma_{12}\\ \sigma_{31}\\ \sigma_{23}\end{bmatrix}
$$

where σ_{ij} are the symmetric Cauchy stresses, ε^{e}_{ij} the elastic strains, c_{ij} the elastic stiffnesses and s_{ij} the elastic compliances.

3. FDM static theory for heterogeneous elasticity and plasticity

3.1. Field equations

The initial static elastic theory of continuously distributed dislocations (ECDD) as initiated by Kröner (1958, 1981), Indenbom (1966), Willis (1967), and reworked by Acharya (2001) includes the following set of field equations (Acharya, 2001; Acharya, 2004; Acharya and Roy, 2006)

$$(3)\qquad \begin{cases} \operatorname{grad}\mathbf{u} = \boldsymbol{\beta} = \boldsymbol{\beta}^{e} + \boldsymbol{\beta}^{p} & \text{(a)} \\ \boldsymbol{\beta}^{e} = \boldsymbol{\beta}^{e}_{\square} + \boldsymbol{\beta}^{e}_{\perp} \;;\; \boldsymbol{\beta}^{p} = \boldsymbol{\beta}^{p}_{\square} + \boldsymbol{\beta}^{p}_{\perp} & \text{(b)} \\ \operatorname{curl}\boldsymbol{\beta}^{e}_{\square} = \operatorname{curl}\boldsymbol{\beta}^{p}_{\square} = 0 & \text{(c)} \\ \boldsymbol{\alpha} = \operatorname{curl}\boldsymbol{\beta}^{e}_{\perp} = -\operatorname{curl}\boldsymbol{\beta}^{p}_{\perp} & \text{(d)} \\ \boldsymbol{\sigma} = \mathbf{C} : \boldsymbol{\varepsilon}^{e} & \text{(e)} \\ \operatorname{div}\boldsymbol{\sigma} = 0 & \text{(f)} \end{cases}$$

where $\mathbf{u}$ is the displacement field and $\boldsymbol{\beta}$ the total distortion field (i.e., the displacement gradient) which decomposes into its elastic $\boldsymbol{\beta}^{e}$ and plastic part $\boldsymbol{\beta}^{p}$ (Eq.(3)a). Due to lattice incompatibility, the elastic and plastic distortion tensors are not gradients and thus not curl free. They have compatible ($\boldsymbol{\beta}^{e}_{\square}$, $\boldsymbol{\beta}^{p}_{\square}$) and incompatible parts ($\boldsymbol{\beta}^{e}_{\perp}$, $\boldsymbol{\beta}^{p}_{\perp}$) (Eq.(3)b). While the compatible part is a gradient and thus curl free (Eq.(3)c), the incompatible part results from geometrically necessary dislocations (GNDs) distribution $\boldsymbol{\alpha}$, and is solution to the incompatibility equation (Eq.(3)d) (see for instance Acharya (2001 or 2004) for a mathematical definition of second-order tensor fields $\mathbf{A}_{\square}$ and $\mathbf{A}_{\perp}$ and the associated unique orthogonal decomposition $\mathbf{A} = \mathbf{A}_{\square} + \mathbf{A}_{\perp}$). As a consequence of the Stokes-Helmholtz decomposition of the elastic and plastic distortions (Eq.(3)d, see also Acharya and Roy (2006)[1] for a more complete description), the incompatible elastic distortion must offset exactly the incompatible plastic distortion to ensure the continuity of matter (i.e. $\boldsymbol{\beta}$ is curl free, Eq.(3)a)

$$(4)\qquad \boldsymbol{\beta}^{e}_{\perp} + \boldsymbol{\beta}^{p}_{\perp} = 0 \;\Leftrightarrow\; \boldsymbol{\beta} = \boldsymbol{\beta}^{e}_{\square} + \boldsymbol{\beta}^{p}_{\square}$$

The stress tensor $\boldsymbol{\sigma}$ is obtained from the tensor of elastic stiffnesses $\mathbf{C}$ (Eqs.(2) and (3)e) and satisfies the static equilibrium equation without body forces (Eq.(3)f). The elastic and plastic strain tensors ($\boldsymbol{\varepsilon}^{e}$, $\boldsymbol{\varepsilon}^{p}$) are the symmetric parts of the elastic and plastic distortion tensors ($\boldsymbol{\beta}^{e}$, $\boldsymbol{\beta}^{p}$), respectively.

3.2. Navier-type equation and incompatibility sources

The fluctuations of elastic moduli $\boldsymbol{\delta}\mathbf{C}(\mathbf{x})$ and of plastic distortions $\boldsymbol{\delta\beta}^{p}(\mathbf{x})$ are now introduced with respect to an infinite homogeneous reference medium $(\mathbf{C}^{0}, \boldsymbol{\beta}^{p0})$ such that the following decompositions hold

$$(5)\qquad \mathbf{C}(\mathbf{x}) = \mathbf{C}^{0} + \boldsymbol{\delta}\mathbf{C}(\mathbf{x}) \;;\; \boldsymbol{\beta}^{p}(\mathbf{x}) = \boldsymbol{\beta}^{p0} + \boldsymbol{\delta\beta}^{p}(\mathbf{x})$$

[1] In Eqs.(3)a-b, Acharya and Roy (2006) explicitly used the following unique Stokes-Helmholtz decomposition for the elastic distortion tensor: $\boldsymbol{\beta}^{e} = \operatorname{grad}(\mathbf{u} - \mathbf{z}) + \boldsymbol{\chi}$ where $\mathbf{u}$ is the total displacement field, $\mathbf{u} - \mathbf{z}$ is a vector field whose gradient forms the compatible part of $\boldsymbol{\beta}^{e}$ (denoted $\boldsymbol{\beta}^{e}_{\square}$) and $\boldsymbol{\chi}$ is the incompatible part of $\boldsymbol{\beta}^{e}$ (denoted $\boldsymbol{\beta}^{e}_{\perp}$) such that $\boldsymbol{\alpha} = \operatorname{curl}\boldsymbol{\chi}$ to be consistent with Eq.(3)d.

Let us anticipate that in the case of a bicrystal, the reference medium will be chosen later to be one of both crystals. Due to the space uniformity of $\boldsymbol{\beta}^{p0}$ in infinite media, its curl is zero so that $\boldsymbol{\beta}^{p0}$ is compatible (its incompatible part $\boldsymbol{\beta}_{\perp}^{p0}$ vanishes). The Stokes-Helmholtz decomposition previously invoked still holds for the fluctuating part $\boldsymbol{\delta\beta}^{p}(\mathbf{x})$:

$$\boldsymbol{\delta\beta}^{p}(\mathbf{x}) = \boldsymbol{\delta\beta}_{\square}^{p}(\mathbf{x}) + \boldsymbol{\delta\beta}_{\perp}^{p}(\mathbf{x}) \tag{6}$$

And the following unique decomposition can be written

$$\boldsymbol{\beta}^{p}(\mathbf{x}) = \boldsymbol{\beta}_{\square}^{p0} + \boldsymbol{\delta\beta}_{\square}^{p}(\mathbf{x}) + \boldsymbol{\delta\beta}_{\perp}^{p}(\mathbf{x}) \tag{7}$$

Eqs.(5) and (7) can be introduced in Eqs.(3)a-f to determine the Navier-type equation

$$\operatorname{div}\left[\left(\mathbf{C}^{0} + \boldsymbol{\delta C}(\mathbf{x})\right) : \left(\operatorname{grad}\mathbf{u}(\mathbf{x}) - \boldsymbol{\beta}_{\square}^{p0} - \boldsymbol{\delta\beta}_{\square}^{p}(\mathbf{x}) - \boldsymbol{\delta\beta}_{\perp}^{p}(\mathbf{x})\right)\right] = 0 \tag{8}$$

which reads

$$\begin{aligned}&\mathbf{C}^{0}\ \operatorname{div}\left(\operatorname{grad}\mathbf{u}(\mathbf{x})\right) - \mathbf{C}^{0}\ \operatorname{div}\boldsymbol{\delta\beta}_{\square}^{p}(\mathbf{x}) - \mathbf{C}^{0}\ \operatorname{div}\boldsymbol{\delta\beta}_{\perp}^{p}(\mathbf{x}) + \operatorname{div}\left(\boldsymbol{\delta C}(\mathbf{x}) : \operatorname{grad}\mathbf{u}(\mathbf{x})\right) - \\ &\operatorname{div}\left(\boldsymbol{\delta C}(\mathbf{x}) : \boldsymbol{\beta}_{\square}^{p0}\right) - \operatorname{div}\left(\boldsymbol{\delta C}(\mathbf{x}) : \boldsymbol{\delta\beta}_{\square}^{p}(\mathbf{x})\right) - \operatorname{div}\left(\boldsymbol{\delta C}(\mathbf{x}) : \boldsymbol{\delta\beta}_{\perp}^{p}(\mathbf{x})\right) = 0\end{aligned} \tag{9}$$

Eq.(9) can be recast as

$$\mathbf{C}^{0}\ \operatorname{div}\left(\operatorname{grad}\mathbf{u}(\mathbf{x})\right) + \mathbf{f}(\mathbf{x}) = 0 \tag{10}$$

where $\mathbf{f}(\mathbf{x}) = \mathbf{f}^{(c)}(\mathbf{x}) + \mathbf{f}^{(i)}(\mathbf{x})$ is the total fictive body force due to incompatibility sources in the material. $\mathbf{f}^{(c)}(\mathbf{x})$ is a fictive body force containing the compatible total distortion ($\operatorname{grad}\mathbf{u}$) and the compatible parts of $\boldsymbol{\beta}^{p}(\mathbf{x})$

$$\begin{aligned}\mathbf{f}^{(c)}(\mathbf{x}) = &\operatorname{div}\left(\boldsymbol{\delta C}(\mathbf{x}) : \operatorname{grad}\mathbf{u}(\mathbf{x})\right) - \mathbf{C}^{0}\ \operatorname{div}\boldsymbol{\delta\beta}_{\square}^{p}(\mathbf{x}) - \operatorname{div}\left(\boldsymbol{\delta C}(\mathbf{x}) : \boldsymbol{\beta}_{\square}^{p0}\right) - \\ &\operatorname{div}\left(\boldsymbol{\delta C}(\mathbf{x}) : \boldsymbol{\delta\beta}_{\square}^{p}(\mathbf{x})\right)\end{aligned} \tag{11}$$

$\mathbf{f}^{(i)}(\mathbf{x})$ is a fictive body force containing the incompatible part of $\boldsymbol{\beta}^{p}(\mathbf{x})$

$$\mathbf{f}^{(i)}(\mathbf{x}) = -\mathbf{C}^{0}\ \operatorname{div}\boldsymbol{\delta\beta}_{\perp}^{p}(\mathbf{x}) - \operatorname{div}\left(\boldsymbol{\delta C}(\mathbf{x}) : \boldsymbol{\delta\beta}_{\perp}^{p}(\mathbf{x})\right) \tag{12}$$

Eqs.(11) and (12) show that the general case where plastic and elastic properties are both heterogeneous give rise to coupling incompatibility effects through $-\operatorname{div}\left(\boldsymbol{\delta C}(\mathbf{x}) : \boldsymbol{\delta\beta}^{p}(\mathbf{x})\right)$. The effects of these elastic-plastic coupling incompatibilities on stresses and elastic rotations will be analyzed and discussed in Section 4 through analytical derivations in the case of an infinite bicrystal with planar boundary and piecewise uniform elastic and plastic properties.

Interestingly, two particular cases can be derived from Eqs.(11),(12). The first case corresponds to homogeneous plastic fields. This case yields $\mathbf{f}^{(i)}(\mathbf{x}) = 0$ and following Eqs.(4), (7) and (11)

$$\mathbf{f}(\mathbf{x}) = \mathbf{f}^{(c)}(\mathbf{x}) = \operatorname{div}\left[\boldsymbol{\delta C}(\mathbf{x}) : \left(\operatorname{grad}\mathbf{u}(\mathbf{x}) - \boldsymbol{\beta}_{\square}^{p0}\right)\right] = \operatorname{div}\left(\boldsymbol{\delta C}(\mathbf{x}) : \boldsymbol{\beta}_{\square}^{e}(\mathbf{x})\right) \tag{13}$$

The second case corresponds to homogeneous elastic properties and yields from Eqs.(6),(11) and (12)

$$\mathbf{f}(\mathbf{x}) = \mathbf{f}^{(c)}(\mathbf{x}) + \mathbf{f}^{(i)}(\mathbf{x}) = -\mathbf{C}^{0}\ \operatorname{div}\boldsymbol{\delta\beta}^{p}(\mathbf{x}) \tag{14}$$

3.3. Burgers vector conservation at surfaces of discontinuity

Let us now consider a fixed plane interface I separating two crystals (crystal I and crystal II) in the current configuration of a continuous medium, with unit normal vector $\mathbf{n}$ oriented from crystal I to crystal II (Fig.1). The limit of continuous fields approaching the interface I from crystal I is assigned the superscript $\boxed{\text{I}}$, and that of fields approaching I from crystal II the superscript $\boxed{\text{II}}$. Hence, the jump of a field $\mathbf{g}$ at a material surface of discontinuity is denoted $[\![\mathbf{g}]\!] = \mathbf{g}^{\boxed{\text{II}}} - \mathbf{g}^{\boxed{\text{I}}}$. Conventional continuum mechanics requires continuity of both the traction vector $\boldsymbol{\sigma}\mathbf{n}$ and the displacement $\mathbf{u}$ across the perfectly bonded interface

(15) $$[\![\boldsymbol{\sigma}]\!]\mathbf{n} = 0 \ ; \ [\![\mathbf{u}]\!] = 0$$

A consequence of the displacement continuity is Hadamard's kinematic compatibility condition (Hadamard, 1903). For small displacements and in the absence of interface motion, it states that

(16) $$[\![\operatorname{grad}\mathbf{u}]\!]\times\mathbf{n} = [\![\boldsymbol{\beta}]\!]\times\mathbf{n} = 0$$

Thus, for any unit vector $\mathbf{t}$ lying in the interface I, Eq.(16) can also be written in the form

(17) $$\forall \mathbf{t} \in I, \ [\![\operatorname{grad}\mathbf{u}]\!]\mathbf{t} = [\![\boldsymbol{\beta}]\!]\mathbf{t} = 0$$

Hadamard's condition reflects the "tangential continuity" of the total distortion $\boldsymbol{\beta}$ across the interface seen as a material surface of discontinuity.

Surfaces of discontinuity such as grain or sub-grain boundaries are conventionally described in terms of surface-dislocations belonging to the interface (Bilby, 1955; Bullough and Bilby, 1956; Christian and Crocker, 1980). The components of the surface-dislocation density tensor $\boldsymbol{\alpha}^{\mathrm{S}}$ in the interface I are expressed as a non-dimensional ratio of a Burgers vector length over a segment length. The surface-dislocations are confined to the interface $\left(\boldsymbol{\alpha}^{\mathrm{S}}\mathbf{n} = 0\right)$ and form a two-dimensional array. For small displacements, they allow accommodation of a discontinuity of the elastic distortion tensor $\boldsymbol{\beta}^{\mathrm{e}}$ across the interface (Beausir et al., 2009; Bilby, 1955; Bullough and Bilby, 1956; Christian and Crocker, 1980; Sutton and Balluffi, 1995)

(18) $$\forall \mathbf{t} \in I, \ \boldsymbol{\alpha}^{\mathrm{S}}\left(\mathbf{n}\times\mathbf{t}\right) = \left[\!\left[\boldsymbol{\beta}^{\mathrm{e}}\right]\!\right]\mathbf{t} \ \text{ or equivalently } \ \boldsymbol{\alpha}^{\mathrm{S}} = -\left[\!\left[\boldsymbol{\beta}^{\mathrm{e}}\right]\!\right]\times\mathbf{n}$$

Eq.(18) can be thought as generalized Frank-Bilby relations (Bilby, 1955; Frank, 1950). Using the standard elastic-plastic decomposition of the total distortion (Eq.(3)(a)) and the Hadamard's condition (Eq.(16)), the surface-dislocations density tensor can also be formulated as

(19) $$\forall \mathbf{t} \in I, \ \boldsymbol{\alpha}^{\mathrm{S}}\left(\mathbf{n}\times\mathbf{t}\right) = -\left[\!\left[\boldsymbol{\beta}^{\mathrm{p}}\right]\!\right]\mathbf{t} \ \text{ or equivalently } \ \boldsymbol{\alpha}^{\mathrm{S}} = \left[\!\left[\boldsymbol{\beta}^{\mathrm{p}}\right]\!\right]\times\mathbf{n}$$

Eqs.(18) and (19) state that any jump in the elastic (or plastic) distortion tensor between the two lattices can be accommodated by an appropriate singular surface-dislocation distribution supported by the interface. Some recent analyses (Acharya, 2007; Acharya et al., 2008; Mach, 2009; Beausir et al., 2009; Mach et al., 2010; Puri et al., 2011; Richeton et al., 2011; Taupin et al., 2012) suggest that a more consistent description of the boundary area can be obtained if continuity of the incompatible elastic (or plastic) displacement across the interface is postulated, i.e. if there is conservation of the Burgers vector content

across the interface (according to Kröner (1981), the true Burgers vector $\mathbf{b}$ of all dislocation lines threading a surface S of the deformed material configuration, surrounded by a contour C is defined for small displacements as $\mathbf{b} = \oint_C \boldsymbol{\beta}^e dx$ (integral form of the incompatibility law)). In such continuous modeling, the boundary area is seen as an extended region supporting a continuous density of bulk GNDs, and the singular description of the incompatibility between crystals through surface-dislocations is surrendered. Hence, the surface-dislocation density tensor is zero and Eqs.(18) and (19) reduce to (Mach, 2009; Beausir et al., 2009; Mach et al., 2010; Puri et al., 2011, Richeton et al., 2011)

$$(20) \qquad \forall \mathbf{t} \in I, \ \begin{cases} \left[\!\left[\boldsymbol{\beta}^{\mathrm{e}} \right]\!\right] \mathbf{t} = 0 \\ \left[\!\left[\boldsymbol{\beta}^{\mathrm{p}} \right]\!\right] \mathbf{t} = 0 \end{cases} \text{ or equivalently } \begin{cases} \left[\!\left[\boldsymbol{\beta}^{\mathrm{e}} \right]\!\right] \times \mathbf{n} = 0 \\ \left[\!\left[\boldsymbol{\beta}^{\mathrm{p}} \right]\!\right] \times \mathbf{n} = 0 \end{cases}$$

4. Analytical derivations for infinite bicrystal with planar boundary

4.1. Piecewise uniform plastic distortions

Here, we follow the static theory of continuously distributed dislocations described in Section 3. The objective is to give the stress fields and lattice misorientations (i.e., elastic rotation jumps) in both crystals of an infinite medium assuming uniform plastic distortion and elastic constants in each crystal. The static configuration is represented in Fig.2 where the infinite grain boundary plane spreads in the (O,x_1,x_3) plane. To be consistent with the Frank-Bilby procedure (Frank, 1950; Bilby, 1955), crystals I and II are separated by the discontinuity interface S with unit normal $\mathbf{n}$ directed toward crystal II from crystal I along the (O,x_2) direction. It is noteworthy that the present calculations would also work for any permutation in the choice of the coordinate axis along the normal to the interface. In consistency with Section 3, the superscript $\boxed{\mathrm{I}}$ is used for fields referring to crystal I and $\boxed{\mathrm{II}}$ for fields referring to crystal II. The static problem of Fig.2 is invariant along (O,x_1) and (O,x_3). As a result, for any field $\mathbf{g}$ referring to the bicrystal properties, we have

$$(21) \qquad \mathbf{g}_{,1} = \mathbf{g}_{,3} = 0$$

The linear theory of small perturbations is considered and the set of field equations set out in Section 3 (Eq.(3)a-f) is solved. In the following, the reference homogeneous infinite medium is chosen as crystal I. Linear elasticity is considered with piecewise uniform elastic moduli

$$(22) \qquad C_{ijkl} = C_{ijkl}^{\boxed{\mathrm{I}}} + \left[\!\left[C_{ijkl} \right]\!\right] H\left(x_2\right)$$

where $H\left(x_2\right)$ is the Heaviside unit step function along (O,x_2)

$$(23) \qquad H\left(x_2\right) = \begin{cases} 1 \text{ if } x_2 > 0 \\ 0 \text{ if } x_2 < 0 \end{cases}$$

The total volume of the bicrystal is denoted V. The bicrystal is submitted to tractions on its external boundary $\mathbf{T} = \boldsymbol{\Sigma}\mathbf{n}_s$, where $\boldsymbol{\Sigma}$ is assumed macro homogeneous and $\mathbf{n}_s$ stands for the outward normal of the external boundary. As previously mentioned, piecewise uniform spatial fluctuations of the plastic distortion components is considered

$$(24) \qquad \beta_{ij}^p = \beta_{ij}^{p\boxed{\mathrm{I}}} + \left[\!\left[\beta_{ij}^p \right]\!\right] H\left(x_2\right)$$

Such assumption is actually equivalent as considering an infinite planar surface-dislocation distribution $\boldsymbol{\alpha}^{\mathrm{S}}$ (and a nil density of polar dislocations $\boldsymbol{\alpha}$ in the bulk). From Eqs.(18) and (19), the surface-dislocations density tensor $\boldsymbol{\alpha}^{\mathrm{S}}$ reads

$$\boldsymbol{\alpha}^{\mathrm{S}} = \begin{pmatrix} \left[\beta^e_{13}\right] & 0 & -\left[\beta^e_{11}\right] \\ \left[\beta^e_{23}\right] & 0 & -\left[\beta^e_{21}\right] \\ \left[\beta^e_{33}\right] & 0 & -\left[\beta^e_{31}\right] \end{pmatrix} = \begin{pmatrix} -\left[\beta^p_{13}\right] & 0 & \left[\beta^p_{11}\right] \\ -\left[\beta^p_{23}\right] & 0 & \left[\beta^p_{21}\right] \\ -\left[\beta^p_{33}\right] & 0 & \left[\beta^p_{31}\right] \end{pmatrix} \tag{25}$$

The full development of the compatibility conditions applied to tensors $\boldsymbol{\beta}^e_{\square}$ and $\boldsymbol{\beta}^p_{\square}$ (Eq.(3)c) is given in Appendix A. Because of the invariance along (O,x_1) and (O,x_3) (Eq.(21)), we have $\boldsymbol{\beta}^e_{\square,1} = \boldsymbol{\beta}^e_{\square,3} = 0$ and $\boldsymbol{\beta}^p_{\square,1} = \boldsymbol{\beta}^p_{\square,3} = 0$. Thus, the compatibility conditions (Eq.(3)) reduce to

$$\forall j \neq 2,\ \left(\beta^e_{\square ij}\right)_{,2} = \left(\beta^p_{\square ij}\right)_{,2} = 0 \tag{26}$$

These equations actually apply to regions where fields are smooth, i.e. for the present situation, respectively in crystal I and in crystal II. At surfaces of discontinuity, they have corresponding jump conditions ($\left[\boldsymbol{\beta}^e_{\square}\right]\times\mathbf{n} = \left[\boldsymbol{\beta}^p_{\square}\right]\times\mathbf{n} = 0$, cf. Eq.(16)). At the interface between crystal I and crystal II, these jump conditions read

$$\forall j \neq 2,\ \left[\beta^e_{\square ij}\right] = \left[\beta^p_{\square ij}\right] = 0 \tag{27}$$

As consequence of Eqs.(26) and (27), for $j \neq 2$, $\beta^e_{\square ij}$ and $\beta^p_{\square ij}$ are thus spatially uniform in the whole bicrystal. Considering Eq.(3)(b), it is hence possible to write

$$\forall j \neq 2,\ \beta^e_{ij} = \beta^e_{\square ij} + \beta^e_{\perp ij} = K'_{ij} + \beta^e_{\perp ij} \tag{28}$$

where K'_{ij} is a spatially uniform function. Then, due to Eqs.(4) and (3)(b), Eq.(28) transforms into

$$\forall j \neq 2,\ \beta^e_{ij} = K'_{ij} - \beta^p_{\perp ij} = K'_{ij} - \left(\beta^p_{ij} - \beta^p_{\square ij}\right) \tag{29}$$

Because for $j \neq 2$, $\beta^p_{\square ij}$ is spatially uniform and because $\boldsymbol{\beta}^{\mathrm{p}}$ is assumed piecewise uniform (Eq.(24)), Eq.(29) can finally be written

$$\forall j \neq 2,\ \beta^e_{ij} = K_{ij} - \left[\beta^p_{ij}\right] H\left(x_2\right) \tag{30}$$

where K_{ij} is another spatially uniform function.

4.1.1. Stresses

4.1.1.1 Heterogeneous anisotropic elasticity

Because of the invariance along (O,x_1) and (O,x_3) (Eq.(21)), stress equilibrium (Eq.(3)f) reduces to $\sigma_{i2,2} = 0$. Besides, self-equilibrium of stresses reads

$$\frac{1}{V}\int_V \sigma_{ij}\, dV = \Sigma_{ij} \tag{31}$$

which actually enforces the condition

(32) $$\sigma_{i2} = \Sigma_{i2}$$

Thus, only the stress components σ_{11}, σ_{33}, σ_{31} are unknown. They are related through the elastic compliances s_{ij} (written in compact notation, see Eq.(2)) to the elastic strains ε_{11}^e, ε_{33}^e, ε_{31}^e

(33) $$\begin{cases} \varepsilon_{11}^e = \beta_{11}^e = s_{11}\sigma_{11} + s_{13}\sigma_{33} + s_{15}\sigma_{31} + \left(s_{12}\Sigma_{22} + s_{14}\Sigma_{12} + s_{16}\Sigma_{23}\right) \\ \varepsilon_{33}^e = \beta_{33}^e = s_{13}\sigma_{11} + s_{33}\sigma_{33} + s_{35}\sigma_{31} + \left(s_{23}\Sigma_{22} + s_{34}\Sigma_{12} + s_{36}\Sigma_{23}\right) \\ 2\varepsilon_{31}^e = \beta_{13}^e + \beta_{31}^e = s_{15}\sigma_{11} + s_{35}\sigma_{33} + s_{55}\sigma_{31} + \left(s_{25}\Sigma_{22} + s_{45}\Sigma_{12} + s_{56}\Sigma_{23}\right) \end{cases}$$

From Eq.(30), the elastic strains ε_{11}^e, ε_{33}^e, ε_{31}^e are uniform piecewise functions. Since the elastic compliances are also uniform piecewise functions, Eq.(33) shows that the stress components are uniform piecewise functions too and can be written

(34) $$\sigma_{ij} = \sigma_{ij}^{\boxed{\text{I}}} + \left[\sigma_{ij}\right] H\left(x_2\right)$$

with $\left[\sigma_{i2}\right] = 0$ from Eq.(32). Furthermore, assuming that the volume fraction of each crystal in the infinite medium is equal (i.e., $V^{\boxed{\text{I}}}/V = V^{\boxed{\text{II}}}/V$), the macroscopic stress reads from Eq.(31)

(35) $$\Sigma_{ij} = \frac{1}{2}\left(\sigma_{ij}^{\boxed{\text{I}}} + \sigma_{ij}^{\boxed{\text{II}}}\right)$$

Substituting the expressions of the elastic distortions given by Eq.(30) into the system Eq.(33), we have

(36) $$\begin{cases} K_{11} - \left[\varepsilon_{11}^p\right] H\left(x_2\right) = s_{11}\sigma_{11} + s_{13}\sigma_{33} + s_{15}\sigma_{31} + \left(s_{12}\Sigma_{22} + s_{14}\Sigma_{12} + s_{16}\Sigma_{23}\right) \\ K_{33} - \left[\varepsilon_{33}^p\right] H\left(x_2\right) = s_{13}\sigma_{11} + s_{33}\sigma_{33} + s_{35}\sigma_{31} + \left(s_{23}\Sigma_{22} + s_{34}\Sigma_{12} + s_{36}\Sigma_{23}\right) \\ K_{13} + K_{31} - 2\left[\varepsilon_{31}^p\right] H\left(x_2\right) = s_{15}\sigma_{11} + s_{35}\sigma_{33} + s_{55}\sigma_{31} + \left(s_{25}\Sigma_{22} + s_{45}\Sigma_{12} + s_{56}\Sigma_{23}\right) \end{cases}$$

It is now possible to derive the expressions of the constant functions K_{ij} by writing the former equations into crystal I ($x_2 < 0$) using Eq.(35)

(37) $$\begin{cases} K_{11} = -\left(s_{11}^{\boxed{\text{I}}}\sigma_{11}^{\boxed{\text{II}}} + s_{13}^{\boxed{\text{I}}}\sigma_{33}^{\boxed{\text{II}}} + s_{15}^{\boxed{\text{I}}}\sigma_{31}^{\boxed{\text{II}}}\right) + 2\left(s_{11}^{\boxed{\text{I}}}\Sigma_{11} + s_{13}^{\boxed{\text{I}}}\Sigma_{33} + s_{15}^{\boxed{\text{I}}}\Sigma_{31}\right) + \left(s_{12}^{\boxed{\text{I}}}\Sigma_{22} + s_{14}^{\boxed{\text{I}}}\Sigma_{12} + s_{16}^{\boxed{\text{I}}}\Sigma_{23}\right) \\ K_{33} = -\left(s_{13}^{\boxed{\text{I}}}\sigma_{11}^{\boxed{\text{II}}} + s_{33}^{\boxed{\text{I}}}\sigma_{33}^{\boxed{\text{II}}} + s_{35}^{\boxed{\text{I}}}\sigma_{31}^{\boxed{\text{II}}}\right) + 2\left(s_{13}^{\boxed{\text{I}}}\Sigma_{11} + s_{33}^{\boxed{\text{I}}}\Sigma_{33} + s_{35}^{\boxed{\text{I}}}\Sigma_{31}\right) + \left(s_{23}^{\boxed{\text{I}}}\Sigma_{22} + s_{34}^{\boxed{\text{I}}}\Sigma_{12} + s_{36}^{\boxed{\text{I}}}\Sigma_{23}\right) \\ K_{13} + K_{31} = -\left(s_{15}^{\boxed{\text{I}}}\sigma_{11}^{\boxed{\text{II}}} + s_{35}^{\boxed{\text{I}}}\sigma_{33}^{\boxed{\text{II}}} + s_{55}^{\boxed{\text{I}}}\sigma_{31}^{\boxed{\text{II}}}\right) + 2\left(s_{15}^{\boxed{\text{I}}}\Sigma_{11} + s_{35}^{\boxed{\text{I}}}\Sigma_{33} + s_{55}^{\boxed{\text{I}}}\Sigma_{31}\right) + \left(s_{25}^{\boxed{\text{I}}}\Sigma_{22} + s_{45}^{\boxed{\text{I}}}\Sigma_{12} + s_{56}^{\boxed{\text{I}}}\Sigma_{23}\right) \end{cases}$$

and into crystal II ($x_2 > 0$)

(38) $$\begin{cases} K_{11} = \left[\varepsilon_{11}^p\right] + s_{11}^{\boxed{\text{II}}}\sigma_{11}^{\boxed{\text{II}}} + s_{13}^{\boxed{\text{II}}}\sigma_{33}^{\boxed{\text{II}}} + s_{15}^{\boxed{\text{II}}}\sigma_{31}^{\boxed{\text{II}}} + \left(s_{12}^{\boxed{\text{II}}}\Sigma_{22} + s_{14}^{\boxed{\text{II}}}\Sigma_{12} + s_{16}^{\boxed{\text{II}}}\Sigma_{23}\right) \\ K_{33} = \left[\varepsilon_{33}^p\right] + s_{13}^{\boxed{\text{II}}}\sigma_{11}^{\boxed{\text{II}}} + s_{33}^{\boxed{\text{II}}}\sigma_{33}^{\boxed{\text{II}}} + s_{35}^{\boxed{\text{II}}}\sigma_{31}^{\boxed{\text{II}}} + \left(s_{23}^{\boxed{\text{II}}}\Sigma_{22} + s_{34}^{\boxed{\text{II}}}\Sigma_{12} + s_{36}^{\boxed{\text{II}}}\Sigma_{23}\right) \\ K_{13} + K_{31} = 2\left[\varepsilon_{31}^p\right] + s_{15}^{\boxed{\text{II}}}\sigma_{11}^{\boxed{\text{II}}} + s_{35}^{\boxed{\text{II}}}\sigma_{33}^{\boxed{\text{II}}} + s_{55}^{\boxed{\text{II}}}\sigma_{31}^{\boxed{\text{II}}} + \left(s_{25}^{\boxed{\text{II}}}\Sigma_{22} + s_{45}^{\boxed{\text{II}}}\Sigma_{12} + s_{56}^{\boxed{\text{II}}}\Sigma_{23}\right) \end{cases}$$

By summing the two expressions of each constant function and by introducing the notation $\tilde{s}_{ij} = s_{ij}^{\boxed{\text{I}}} + s_{ij}^{\boxed{\text{II}}}$, the system writes also

$$(39)\quad \begin{cases} K_{11} = \dfrac{1}{2}\left(\left[\varepsilon_{11}^{p}\right] + \left[s_{11}\right]\sigma_{11}^{\boxed{II}} + \left[s_{13}\right]\sigma_{33}^{\boxed{II}} + \left[s_{15}\right]\sigma_{31}^{\boxed{II}} + \tilde{s}_{12}\Sigma_{22} + \tilde{s}_{14}\Sigma_{12} + \tilde{s}_{16}\Sigma_{23}\right) + \left(s_{11}^{\boxed{I}}\Sigma_{11} + s_{13}^{\boxed{I}}\Sigma_{33} + s_{15}^{\boxed{I}}\Sigma_{31}\right) \\ K_{33} = \dfrac{1}{2}\left(\left[\varepsilon_{33}^{p}\right] + \left[s_{13}\right]\sigma_{11}^{\boxed{II}} + \left[s_{33}\right]\sigma_{33}^{\boxed{II}} + \left[s_{35}\right]\sigma_{31}^{\boxed{II}} + \tilde{s}_{23}\Sigma_{22} + \tilde{s}_{34}\Sigma_{12} + \tilde{s}_{36}\Sigma_{23}\right) + \left(s_{13}^{\boxed{I}}\Sigma_{11} + s_{33}^{\boxed{I}}\Sigma_{33} + s_{35}^{\boxed{I}}\Sigma_{31}\right) \\ K_{13} + K_{31} = \left[\varepsilon_{31}^{p}\right] + \dfrac{1}{2}\left(s_{15}\sigma_{11}^{\boxed{II}} + s_{35}\sigma_{33}^{\boxed{II}} + s_{55}\sigma_{31}^{\boxed{II}} + \tilde{s}_{25}\Sigma_{22} + \tilde{s}_{45}\Sigma_{12} + \tilde{s}_{56}\Sigma_{23}\right) + \left(s_{15}^{\boxed{I}}\Sigma_{11} + s_{35}^{\boxed{I}}\Sigma_{33} + s_{55}^{\boxed{I}}\Sigma_{31}\right) \end{cases}$$

From Eq.(33), the unknown elastic distortion components in crystal II are expressed as

$$(40)\quad \begin{cases} \varepsilon_{11}^{e\,\boxed{II}} = s_{11}^{\boxed{II}}\sigma_{11}^{\boxed{II}} + s_{13}^{\boxed{II}}\sigma_{33}^{\boxed{II}} + s_{15}^{\boxed{II}}\sigma_{31}^{\boxed{II}} + \left(s_{12}^{\boxed{II}}\Sigma_{22} + s_{14}^{\boxed{II}}\Sigma_{12} + s_{16}^{\boxed{II}}\Sigma_{23}\right) \\ \varepsilon_{33}^{e\,\boxed{II}} = s_{13}^{\boxed{II}}\sigma_{11}^{\boxed{II}} + s_{33}^{\boxed{II}}\sigma_{33}^{\boxed{II}} + s_{35}^{\boxed{II}}\sigma_{31}^{\boxed{II}} + \left(s_{23}^{\boxed{II}}\Sigma_{22} + s_{34}^{\boxed{II}}\Sigma_{12} + s_{36}^{\boxed{II}}\Sigma_{23}\right) \\ 2\varepsilon_{31}^{e\,\boxed{II}} = s_{15}^{\boxed{II}}\sigma_{11}^{\boxed{II}} + s_{35}^{\boxed{II}}\sigma_{33}^{\boxed{II}} + s_{55}^{\boxed{II}}\sigma_{31}^{\boxed{II}} + \left(s_{25}^{\boxed{II}}\Sigma_{22} + s_{45}^{\boxed{II}}\Sigma_{12} + s_{56}^{\boxed{II}}\Sigma_{23}\right) \end{cases}$$

and from Eqs.(30) and (39) they also read

$$(41)\quad \begin{cases} \varepsilon_{11}^{e\,\boxed{II}} = \dfrac{1}{2}\left(-\left[\varepsilon_{11}^{p}\right] + \left[s_{11}\right]\sigma_{11}^{\boxed{II}} + \left[s_{13}\right]\sigma_{33}^{\boxed{II}} + \left[s_{15}\right]\sigma_{31}^{\boxed{II}}\right) + \dfrac{1}{2}\left(\tilde{s}_{12}\Sigma_{22} + \tilde{s}_{14}\Sigma_{12} + \tilde{s}_{16}\Sigma_{23}\right) + \left(s_{11}^{\boxed{I}}\Sigma_{11} + s_{13}^{\boxed{I}}\Sigma_{33} + s_{15}^{\boxed{I}}\Sigma_{31}\right) \\ \varepsilon_{33}^{e\,\boxed{II}} = \dfrac{1}{2}\left(-\left[\varepsilon_{33}^{p}\right] + \left[s_{13}\right]\sigma_{11}^{\boxed{II}} + \left[s_{33}\right]\sigma_{33}^{\boxed{II}} + \left[s_{35}\right]\sigma_{31}^{\boxed{II}}\right) + \dfrac{1}{2}\left(\tilde{s}_{23}\Sigma_{22} + \tilde{s}_{34}\Sigma_{12} + \tilde{s}_{36}\Sigma_{23}\right) + \left(s_{13}^{\boxed{I}}\Sigma_{11} + s_{33}^{\boxed{I}}\Sigma_{33} + s_{35}^{\boxed{I}}\Sigma_{31}\right) \\ 2\varepsilon_{31}^{e\,\boxed{II}} = \dfrac{1}{2}\left(-2\left[\varepsilon_{31}^{p}\right] + \left[s_{15}\right]\sigma_{11}^{\boxed{II}} + \left[s_{35}\right]\sigma_{33}^{\boxed{II}} + \left[s_{55}\right]\sigma_{31}^{\boxed{II}}\right) + \dfrac{1}{2}\left(\tilde{s}_{25}\Sigma_{22} + \tilde{s}_{45}\Sigma_{12} + \tilde{s}_{56}\Sigma_{23}\right) + \left(s_{15}^{\boxed{I}}\Sigma_{11} + s_{35}^{\boxed{I}}\Sigma_{33} + s_{55}^{\boxed{I}}\Sigma_{31}\right) \end{cases}$$

The combination of Eqs.(40) and (41) leads then to the following linear system

$$(42)\quad \begin{cases} \tilde{s}_{11}\sigma_{11}^{\boxed{II}} + \tilde{s}_{13}\sigma_{33}^{\boxed{II}} + \tilde{s}_{15}\sigma_{31}^{\boxed{II}} = -\left(\left[\varepsilon_{11}^{p}\right] + \left[s_{12}\right]\Sigma_{22} + \left[s_{14}\right]\Sigma_{12} + \left[s_{16}\right]\Sigma_{23}\right) + 2\left(s_{11}^{\boxed{I}}\Sigma_{11} + s_{13}^{\boxed{I}}\Sigma_{33} + s_{15}^{\boxed{I}}\Sigma_{31}\right) \\ \tilde{s}_{13}\sigma_{11}^{\boxed{II}} + \tilde{s}_{33}\sigma_{33}^{\boxed{II}} + \tilde{s}_{35}\sigma_{31}^{\boxed{II}} = -\left(\left[\varepsilon_{33}^{p}\right] + \left[s_{23}\right]\Sigma_{22} + \left[s_{34}\right]\Sigma_{12} + \left[s_{36}\right]\Sigma_{23}\right) + 2\left(s_{13}^{\boxed{I}}\Sigma_{11} + s_{33}^{\boxed{I}}\Sigma_{33} + s_{35}^{\boxed{I}}\Sigma_{31}\right) \\ \tilde{s}_{15}\sigma_{11}^{\boxed{II}} + \tilde{s}_{35}\sigma_{33}^{\boxed{II}} + \tilde{s}_{55}\sigma_{31}^{\boxed{II}} = -\left(2\left[\varepsilon_{31}^{p}\right] + \left[s_{25}\right]\Sigma_{22} + \left[s_{45}\right]\Sigma_{12} + \left[s_{56}\right]\Sigma_{23}\right) + 2\left(s_{15}^{\boxed{I}}\Sigma_{11} + s_{35}^{\boxed{I}}\Sigma_{33} + s_{55}^{\boxed{I}}\Sigma_{31}\right) \end{cases}$$

The expressions of the stress components in crystal II follow directly from the resolution of this linear system of 3 equations with 3 unknowns. Then the stresses in crystal I are given from Eq.(35) by

$$(43)\quad \sigma_{ij}^{\boxed{I}} = 2\Sigma_{ij} - \sigma_{ij}^{\boxed{II}}$$

Let us now adopt the following notations

$$(44)\quad \begin{cases} \left[\varepsilon_{11}^{*}\right] = \left[\varepsilon_{11}^{p}\right] + \left[s_{12}\right]\Sigma_{22} + \left[s_{14}\right]\Sigma_{12} + \left[s_{16}\right]\Sigma_{23} - 2\left(s_{11}^{\boxed{I}}\Sigma_{11} + s_{13}^{\boxed{I}}\Sigma_{33} + s_{15}^{\boxed{I}}\Sigma_{31}\right) \\ \left[\varepsilon_{33}^{*}\right] = \left[\varepsilon_{33}^{p}\right] + \left[s_{23}\right]\Sigma_{22} + \left[s_{34}\right]\Sigma_{12} + \left[s_{36}\right]\Sigma_{23} - 2\left(s_{13}^{\boxed{I}}\Sigma_{11} + s_{33}^{\boxed{I}}\Sigma_{33} + s_{35}^{\boxed{I}}\Sigma_{31}\right) \\ 2\left[\varepsilon_{31}^{*}\right] = 2\left[\varepsilon_{31}^{p}\right] + \left[s_{25}\right]\Sigma_{22} + \left[s_{45}\right]\Sigma_{12} + \left[s_{56}\right]\Sigma_{23} - 2\left(s_{15}^{\boxed{I}}\Sigma_{11} + s_{35}^{\boxed{I}}\Sigma_{33} + s_{55}^{\boxed{I}}\Sigma_{31}\right) \end{cases}$$

In the general case of piecewise uniform anisotropic elasticity with non zero macroscopic stress, we have then

$$
(45)\qquad
\begin{cases}
\sigma_{11}^{\boxed{II}} = \dfrac{\left(\tilde{s}_{33}\tilde{s}_{55}-\tilde{s}_{35}{}^{2}\right)\left[\varepsilon_{11}^{*}\right]-\left(\tilde{s}_{13}\tilde{s}_{55}-\tilde{s}_{15}\tilde{s}_{35}\right)\left[\varepsilon_{33}^{*}\right]+2\left(\tilde{s}_{13}\tilde{s}_{35}-\tilde{s}_{33}\tilde{s}_{15}\right)\left[\varepsilon_{31}^{*}\right]}{\tilde{s}_{11}\tilde{s}_{35}{}^{2}+\tilde{s}_{33}\tilde{s}_{15}{}^{2}+\tilde{s}_{55}\tilde{s}_{13}{}^{2}-\tilde{s}_{11}\tilde{s}_{33}\tilde{s}_{55}-2\tilde{s}_{13}\tilde{s}_{15}\tilde{s}_{35}} \\
\sigma_{33}^{\boxed{II}} = \dfrac{-\left(\tilde{s}_{13}\tilde{s}_{55}-\tilde{s}_{15}\tilde{s}_{35}\right)\left[\varepsilon_{11}^{*}\right]+\left(\tilde{s}_{11}\tilde{s}_{55}-\tilde{s}_{15}{}^{2}\right)\left[\varepsilon_{33}^{*}\right]+2\left(\tilde{s}_{13}\tilde{s}_{15}-\tilde{s}_{11}\tilde{s}_{35}\right)\left[\varepsilon_{31}^{*}\right]}{\tilde{s}_{11}\tilde{s}_{35}{}^{2}+\tilde{s}_{33}\tilde{s}_{15}{}^{2}+\tilde{s}_{55}\tilde{s}_{13}{}^{2}-\tilde{s}_{11}\tilde{s}_{33}\tilde{s}_{55}-2\tilde{s}_{13}\tilde{s}_{15}\tilde{s}_{35}} \\
\sigma_{31}^{\boxed{II}} = \dfrac{\left(\tilde{s}_{13}\tilde{s}_{35}-\tilde{s}_{33}\tilde{s}_{15}\right)\left[\varepsilon_{11}^{*}\right]+\left(\tilde{s}_{13}\tilde{s}_{15}-\tilde{s}_{11}\tilde{s}_{35}\right)\left[\varepsilon_{33}^{*}\right]+2\left(\tilde{s}_{11}\tilde{s}_{33}-\tilde{s}_{13}{}^{2}\right)\left[\varepsilon_{31}^{*}\right]}{\tilde{s}_{11}\tilde{s}_{35}{}^{2}+\tilde{s}_{33}\tilde{s}_{15}{}^{2}+\tilde{s}_{55}\tilde{s}_{13}{}^{2}-\tilde{s}_{11}\tilde{s}_{33}\tilde{s}_{55}-2\tilde{s}_{13}\tilde{s}_{15}\tilde{s}_{35}}
\end{cases}
$$

It is interesting to notice that these solutions are independent of compliances s_{22}, s_{24}, s_{26}, s_{44}, s_{46}, s_{66} and of plastic strains ε_{12}^{p}, ε_{22}^{p}, ε_{23}^{p}. It can be seen that the stresses contain different sources of incompatibilities as highlighted in the general static FDM theory considered in Section 3.2. If one writes $\tilde{s}_{ij} = 2s_{ij}^{\boxed{I}} + \left[s_{ij}\right]$ and considers crystal I as the reference medium, it is indeed possible to decompose the stress field into the following way

$$
(46)\qquad \sigma_{ij} = \Sigma_{ij} + \sigma_{ij}^{\Delta\mathbf{s}} + \sigma_{ij}^{\Delta\boldsymbol{\varepsilon}^{\mathrm{p}}} + \sigma_{ij}^{\Delta\mathbf{s}\Delta\boldsymbol{\varepsilon}^{\mathrm{p}}}
$$

with

- $\Sigma_{ij} = \sigma_{ij}\left(\left[\mathbf{s}\right]=\left[\boldsymbol{\varepsilon}^{\mathrm{p}}\right]=\mathbf{0}\right)$, resulting term when all sources of incompatibilities are set to zero (in this case, one rightly retrieves that the stress equals the macroscopic uniform stress),
- $\sigma_{ij}^{\Delta\mathbf{s}} = \sigma_{ij}\left(\left[\boldsymbol{\varepsilon}^{\mathrm{p}}\right]=\mathbf{0}\right) - \Sigma_{ij}$, internal stress term due to elastic incompatibilities alone $\left(\Delta\mathbf{s}\right)$,
- $\sigma_{ij}^{\Delta\boldsymbol{\varepsilon}^{\mathrm{p}}} = \sigma_{ij}\left(\left[\mathbf{s}\right]=\mathbf{0}\right) - \Sigma_{ij}$, internal stress term due to plastic incompatibilities alone ($\Delta\boldsymbol{\varepsilon}^{\mathrm{p}}$),
- $\sigma_{ij}^{\Delta\mathbf{s}\Delta\boldsymbol{\varepsilon}^{\mathrm{p}}} = \sigma_{ij} - \left(\Sigma_{ij} + \sigma_{ij}^{\Delta\mathbf{s}} + \sigma_{ij}^{\Delta\boldsymbol{\varepsilon}^{\mathrm{p}}}\right)$, internal stress term due to couplings between elastic and plastic incompatibilities $\left(\Delta\mathbf{s}\Delta\boldsymbol{\varepsilon}^{\mathrm{p}}\right)$.

4.1.1.2 Heterogeneous isotropic elasticity

In the case of piecewise uniform isotropic elasticity (i.e heterogeneous elasticity) characterized for crystal I (resp. crystal II) by Young modulus $E^{\boxed{I}}$ (resp. $E^{\boxed{II}}$) and Poisson's ratio $\nu^{\boxed{I}}$ (resp. $\nu^{\boxed{II}}$) with shear modulus $\mu^{\boxed{I}} = \dfrac{E^{\boxed{I}}}{2\left(1+\nu^{\boxed{I}}\right)}$ (resp. $\mu^{\boxed{II}} = \dfrac{E^{\boxed{II}}}{2\left(1+\nu^{\boxed{II}}\right)}$), the system of Eq.(42) reads

(47)
$$\begin{cases} \left(\frac{1}{E^{\boxed{I}}}+\frac{1}{E^{\boxed{II}}}\right)\sigma_{11}-\left(\frac{\nu^{\boxed{I}}}{E^{\boxed{I}}}+\frac{\nu^{\boxed{II}}}{E^{\boxed{II}}}\right)\sigma_{33}=-\left[\varepsilon_{11}^{p}\right]+\left(\frac{\nu^{\boxed{II}}}{E^{\boxed{II}}}-\frac{\nu^{\boxed{I}}}{E^{\boxed{I}}}\right)\Sigma_{22}+\frac{2}{E^{\boxed{I}}}\Sigma_{11}-\frac{2\nu^{\boxed{I}}}{E^{\boxed{I}}}\Sigma_{33} \\ -\left(\frac{\nu^{\boxed{I}}}{E^{\boxed{I}}}+\frac{\nu^{\boxed{II}}}{E^{\boxed{II}}}\right)\sigma_{11}+\left(\frac{1}{E^{\boxed{I}}}+\frac{1}{E^{\boxed{II}}}\right)\sigma_{33}=-\left[\varepsilon_{33}^{p}\right]+\left(\frac{\nu^{\boxed{II}}}{E^{\boxed{II}}}-\frac{\nu^{\boxed{I}}}{E^{\boxed{I}}}\right)\Sigma_{22}-\frac{2\nu^{\boxed{I}}}{E^{\boxed{I}}}\Sigma_{11}+\frac{2}{E^{\boxed{I}}}\Sigma_{33} \\ \left(\frac{1}{\mu^{\boxed{I}}}+\frac{1}{\mu^{\boxed{II}}}\right)\sigma_{31}=-2\left[\varepsilon_{31}^{p}\right]+\frac{2}{\mu^{\boxed{I}}}\Sigma_{31} \end{cases}$$

and its resolution leads to the following solutions

(48)
$$\begin{cases} \sigma_{11}^{\boxed{II}}=\dfrac{\left(\frac{\nu^{\boxed{I}}}{E^{\boxed{I}}}+\frac{\nu^{\boxed{II}}}{E^{\boxed{II}}}\right)\left[\varepsilon_{33}^{p}\right]+\left(\frac{1}{E^{\boxed{I}}}+\frac{1}{E^{\boxed{II}}}\right)\left[\varepsilon_{11}^{p}\right]-\frac{1}{2}\left(\frac{1}{\mu^{\boxed{I}}}+\frac{1}{\mu^{\boxed{II}}}\right)\left(\frac{\nu^{\boxed{II}}}{E^{\boxed{II}}}-\frac{\nu^{\boxed{I}}}{E^{\boxed{I}}}\right)\Sigma_{22}+\left(\frac{\nu^{\boxed{I}}-1}{\mu^{\boxed{I}}E^{\boxed{I}}}+\frac{2\left(\nu^{\boxed{I}}\nu^{\boxed{II}}-1\right)}{E^{\boxed{I}}E^{\boxed{II}}}\right)\Sigma_{11}+\frac{2\left(\nu^{\boxed{I}}-\nu^{\boxed{II}}\right)}{E^{\boxed{I}}E^{\boxed{II}}}\Sigma_{33}}{\left(\frac{\nu^{\boxed{I}}}{E^{\boxed{I}}}+\frac{\nu^{\boxed{II}}}{E^{\boxed{II}}}\right)^{2}-\left(\frac{1}{E^{\boxed{I}}}+\frac{1}{E^{\boxed{II}}}\right)^{2}} \\ \sigma_{33}^{\boxed{II}}=\dfrac{\left(\frac{\nu^{\boxed{I}}}{E^{\boxed{I}}}+\frac{\nu^{\boxed{II}}}{E^{\boxed{II}}}\right)\left[\varepsilon_{11}^{p}\right]+\left(\frac{1}{E^{\boxed{I}}}+\frac{1}{E^{\boxed{II}}}\right)\left[\varepsilon_{33}^{p}\right]-\frac{1}{2}\left(\frac{1}{\mu^{\boxed{I}}}+\frac{1}{\mu^{\boxed{II}}}\right)\left(\frac{\nu^{\boxed{II}}}{E^{\boxed{II}}}-\frac{\nu^{\boxed{I}}}{E^{\boxed{I}}}\right)\Sigma_{22}+\left(\frac{\nu^{\boxed{I}}-1}{\mu^{\boxed{I}}E^{\boxed{I}}}+\frac{2\left(\nu^{\boxed{I}}\nu^{\boxed{II}}-1\right)}{E^{\boxed{I}}E^{\boxed{II}}}\right)\Sigma_{33}+\frac{2\left(\nu^{\boxed{I}}-\nu^{\boxed{II}}\right)}{E^{\boxed{I}}E^{\boxed{II}}}\Sigma_{11}}{\left(\frac{\nu^{\boxed{I}}}{E^{\boxed{I}}}+\frac{\nu^{\boxed{II}}}{E^{\boxed{II}}}\right)^{2}-\left(\frac{1}{E^{\boxed{I}}}+\frac{1}{E^{\boxed{II}}}\right)^{2}} \\ \sigma_{31}^{\boxed{II}}=-\frac{2\mu^{\boxed{I}}\mu^{\boxed{II}}}{\mu^{\boxed{I}}+\mu^{\boxed{II}}}\left[\varepsilon_{31}^{p}\right]+\frac{2\mu^{\boxed{II}}}{\mu^{\boxed{I}}+\mu^{\boxed{II}}}\Sigma_{31} \end{cases}$$

4.1.1.3 Homogeneous isotropic elasticity

In the case of homogeneous and isotropic elasticity now characterized by uniform Young modulus $E=E^{\boxed{I}}=E^{\boxed{II}}$ and uniform Poisson's ratio $\nu=\nu^{\boxed{I}}=\nu^{\boxed{II}}$ (the shear modulus being given by $\mu=\mu^{\boxed{I}}=\mu^{\boxed{II}}=\dfrac{E}{2(1+\nu)}$), Eq.(48) simplifies to

(49)
$$\begin{cases} \sigma_{11}^{\boxed{II}}=\Sigma_{11}-\dfrac{\mu}{1-\nu}\left(\left[\varepsilon_{11}^{p}\right]+\nu\left[\varepsilon_{33}^{p}\right]\right) \\ \sigma_{33}^{\boxed{II}}=\Sigma_{33}-\dfrac{\mu}{1-\nu}\left(\left[\varepsilon_{33}^{p}\right]+\nu\left[\varepsilon_{11}^{p}\right]\right) \\ \sigma_{31}^{\boxed{II}}=\Sigma_{31}-\mu\left[\varepsilon_{31}^{p}\right] \end{cases}$$

Finally, using Eq.(35) we have

(50)
$$\begin{cases} \sigma_{11}=\Sigma_{11}-\dfrac{\mu}{1-\nu}\left(\left[\varepsilon_{11}^{p}\right]+\nu\left[\varepsilon_{33}^{p}\right]\right)\mathrm{sgn}\left(x_2\right) \\ \sigma_{33}=\Sigma_{33}-\dfrac{\mu}{1-\nu}\left(\left[\varepsilon_{33}^{p}\right]+\nu\left[\varepsilon_{11}^{p}\right]\right)\mathrm{sgn}\left(x_2\right) \\ \sigma_{31}=\Sigma_{31}-\mu\left[\varepsilon_{31}^{p}\right]\mathrm{sgn}\left(x_2\right) \end{cases}$$

where $\mathrm{sgn}\left(x_2\right)=1$ when $x_2>0$ (i.e. in crystal II following Fig.2) and $\mathrm{sgn}\left(x_2\right)=-1$ when $x_2<0$ (i.e. in crystal I).

4.1.1.4 Comparison with other works and techniques

To the authors' knowledge, the explicit stress formula obtained in the general context of heterogeneous anisotropic elasticity with plastic strains (Eq.(45)) had never been formulated in a closed-form solution before. However, the explicit expression in the particular case of isotropic elasticity (Eq.(50)) was already derived by other techniques: Fourier transforms (Rey and Saada, 1976), second order Beltrami stress function (see Kröner, 1981) for plane problems in the real space (Berveiller, 1978; Rey and Zaoui, 1980) or from consideration of boundary conditions for stresses and compatibility conditions for strains at the interface (Gemperlova et al., 1989). Note however that the present calculations do not require the assumption of plastic incompressibility (i.e. our calculations are also valid in the case of dilatant plasticity) in contrast with the calculations performed by Berveiller (1978). Furthermore, it is noteworthy that the linear system of equations (Eq.(42)) giving the full solutions was actually written by Gemperlova et al. (1989) for the most general case. It can be noted however that the form is somewhat different than in Eq.(42) and that there is a typographic error in the published expression. A correct expression can be found in the book of Sutton and Ballufi (1995, p.707). Gemperlova et al. (1989) also formulated the solution in the case of heterogeneous isotropic elasticity and found expressions equivalent to Eq.(48) (Sutton and Ballufi, 1995). The most noticeable difference between the approach of Gemperlova et al. (1989) and the present one is that they consider boundary conditions for stresses and compatibility conditions for strains at the interface whereas we consider stress equilibrium and the compatibility conditions for $\boldsymbol{\beta}^{e}_{\square}$ and $\boldsymbol{\beta}^{p}_{\square}$ in the bulk (Eq.(28)). Hence, the proof is given from Eq.(30) that elastic strains and stresses are piecewise uniform functions whereas it is an implicit assumption in the work of Gemperlova et al. (1989).

Besides, Eq.(45) can also be derived in terms of elastic stress concentration and influence tensors following the homogenization techniques described in Stupkiewicz and Petryk (2002), and in Franciosi and Berbenni (2007, 2008). Thus, after some algebra manipulations on these tensors, we can recast the stresses as follows

$$\begin{cases} \sigma_P^{\boxed{II}} = B_{PP'}^{\boxed{II}} \Sigma_{P'} + B_{PA}^{\boxed{II}} \Sigma_A + F_{PP'} \left[\varepsilon_{P'}^p \right] \\ \sigma_P^{\boxed{I}} = B_{PP'}^{\boxed{I}} \Sigma_{P'} + B_{PA}^{\boxed{I}} \Sigma_A - F_{PP'} \left[\varepsilon_{P'}^p \right] \end{cases} \tag{51}$$

where P, P' denote plane components 11, 33, 13 (corresponding resp. to 1, 3, 5 in the reduction convention settled by Eq.(2)), and A denotes anti-plane components 22, 12, 23 (resp. 2, 4, 6 in the reduction convention) and $\left[\varepsilon_P^p \right] = \begin{pmatrix} \left[\varepsilon_{11}^p \right] \\ \left[\varepsilon_{33}^p \right] \\ 2\left[\varepsilon_{13}^p \right] \end{pmatrix}$. $B_{PP'}^{\boxed{I}}$ (resp. $B_{PP'}^{\boxed{II}}$), $B_{PA}^{\boxed{I}}$ (resp. $B_{PA}^{\boxed{II}}$) are the elastic stress concentration tensors for crystal I (resp. crystal II), and $F_{PP'}$ is the non zero part of the elastic stress influence tensor. From overall stress equilibrium (Eq.(35)), the elastic stress concentration tensors verify

$$\begin{cases} \dfrac{B_{PP'}^{\boxed{I}} + B_{PP'}^{\boxed{II}}}{2} = I_{PP'} \\ \dfrac{B_{PA}^{\boxed{I}} + B_{PA}^{\boxed{II}}}{2} = 0 \end{cases} \tag{52}$$

with $I_{PP'}$ the PP' part of the unit tensor I_{ijkl}. So, finally Eq.(50) simplifies to

$$\begin{cases} \sigma_P^{\boxed{\text{II}}} = B_{PP'}^{\boxed{\text{II}}} \Sigma_{P'} + B_{PA}^{\boxed{\text{II}}} \Sigma_A + F_{PP'} \left[\varepsilon_{P'}^p \right] \\ \sigma_P^{\boxed{\text{I}}} = \left(2I_{PP'} - B_{PP'}^{\boxed{\text{II}}} \right) \Sigma_{P'} - B_{PA}^{\boxed{\text{II}}} \Sigma_A - F_{PP'} \left[\varepsilon_{P'}^p \right] \end{cases} \tag{53}$$

The expressions for the components of $B_{PP'}^{\boxed{\text{II}}}$, $B_{PA}^{\boxed{\text{II}}}$ and $F_{PP'}$ are obtained from the explicit Eq.(45) and are given in Appendix B. Using the general homogenization technique recently developed in Stupkiewicz and Petryk (2002), Franciosi and Berbenni (2007, 2008), the explicit formulas for bicrystals with general elastic anisotropy are given by Eq.(53) together with Eqs.(B.1), (B.2) and (B.3). These explicit formulas were not reported in the literature to our knowledge.

4.1.2. Elastic energy density

The volume density of elastic energy is computed as

$$\varphi = \frac{1}{2} \sigma_{ij} \varepsilon_{ij}^e \tag{54}$$

where the elastic strains ε_{ij}^e can be deduced from the Hooke's law (Eq.(2)). Thus

$$\varphi = \frac{1}{2} \sigma_{ij} s_{ijkl} \sigma_{kl} \tag{55}$$

where σ_{ij} are given by Eqs.(43) and (45) for both crystals.

4.1.3. Lattice rotations

4.1.3.1 Heterogeneous anisotropic elasticity

The lattice rotations are linked to the elastic rotation $\boldsymbol{\omega}^{\mathrm{e}}$, defined as the skew-symmetric part of the elastic distortion tensor

$$\boldsymbol{\omega}^{\mathrm{e}} = \frac{1}{2} \left(\boldsymbol{\beta}^{\mathrm{e}} - \left(\boldsymbol{\beta}^{\mathrm{e}} \right)^{\mathrm{T}} \right) \tag{56}$$

In addition, the equivalent elastic rotation vector $\boldsymbol{\Omega}^{\mathrm{e}}$ is introduced such that

$$\forall \mathbf{l}, \quad \boldsymbol{\omega}^{\mathrm{e}} \mathbf{l} = \boldsymbol{\Omega}^{\mathrm{e}} \times \mathbf{l} \tag{57}$$

In the following, only an analytical formula for its jump, $\left[\boldsymbol{\Omega}^{\mathrm{e}} \right]$, is derived, which allows giving further insights on the lattice misorientation angle between two crystals, assuming their initial orientation is known. From Eq.(25), the jump of the tangential elastic distortions is known

$$\forall j \neq 2, \left[\beta_{ij}^e \right] = -\left[\beta_{ij}^p \right] \tag{58}$$

The normal components can be deduced from the jump of elastic strains which are known from the Hooke's law (Eq.(2)). In particular, we have

$$\begin{cases} \left[\beta_{12}^e \right] = 2 \left[\varepsilon_{12}^e \right] - \left[\beta_{21}^e \right] = 2 \left[\varepsilon_{12}^e \right] + \left[\beta_{21}^p \right] \\ \left[\beta_{32}^e \right] = 2 \left[\varepsilon_{23}^e \right] - \left[\beta_{23}^e \right] = 2 \left[\varepsilon_{23}^e \right] + \left[\beta_{23}^p \right] \end{cases} \tag{59}$$

Then the jumps of lattice rotations are accordingly derived

(60)
$$\begin{cases} \left[\Omega_1^e\right] = -\left[\omega_{23}^e\right] = \left[\varepsilon_{23}^e\right] + \left[\beta_{23}^p\right] \\ \left[\Omega_2^e\right] = \left[\omega_{13}^e\right] = \frac{1}{2}\left(\left[\beta_{31}^p\right] - \left[\beta_{13}^p\right]\right) \\ \left[\Omega_3^e\right] = -\left[\omega_{12}^e\right] = -\left(\left[\varepsilon_{12}^e\right] + \left[\beta_{21}^p\right]\right) \end{cases}$$

with

(61)
$$\begin{cases} 2\left[\varepsilon_{12}^e\right] = 2\left(s_{14}^{\boxed{\mathrm{I}}}\left(\sigma_{11}^{\boxed{\mathrm{II}}} - \Sigma_{11}\right) + s_{34}^{\boxed{\mathrm{I}}}\left(\sigma_{33}^{\boxed{\mathrm{II}}} - \Sigma_{33}\right) + s_{45}^{\boxed{\mathrm{I}}}\left(\sigma_{31}^{\boxed{\mathrm{II}}} - \Sigma_{31}\right)\right) \\ + \left[s_{14}\right]\sigma_{11}^{\boxed{\mathrm{II}}} + \left[s_{34}\right]\sigma_{33}^{\boxed{\mathrm{II}}} + \left[s_{45}\right]\sigma_{31}^{\boxed{\mathrm{II}}} + \left[s_{24}\right]\Sigma_{22} + \left[s_{44}\right]\Sigma_{12} + \left[s_{46}\right]\Sigma_{23} \\ 2\left[\varepsilon_{23}^e\right] = 2\left(s_{16}^{\boxed{\mathrm{I}}}\left(\sigma_{11}^{\boxed{\mathrm{II}}} - \Sigma_{11}\right) + s_{36}^{\boxed{\mathrm{I}}}\left(\sigma_{33}^{\boxed{\mathrm{II}}} - \Sigma_{33}\right) + s_{46}^{\boxed{\mathrm{I}}}\left(\sigma_{31}^{\boxed{\mathrm{II}}} - \Sigma_{31}\right)\right) \\ + \left[s_{16}\right]\sigma_{11}^{\boxed{\mathrm{II}}} + \left[s_{36}\right]\sigma_{33}^{\boxed{\mathrm{II}}} + \left[s_{56}\right]\sigma_{31}^{\boxed{\mathrm{II}}} + \left[s_{26}\right]\Sigma_{22} + \left[s_{46}\right]\Sigma_{12} + \left[s_{66}\right]\Sigma_{23} \end{cases}$$

In comparison with the stresses, the present solutions are only independent of compliance s_{22} and of plastic distortions β_{12}^p, β_{22}^p, β_{32}^p. It is also possible to decompose the elastic rotation vector jump components into the following way

(62)
$$\left[\Omega_i^e\right] = \left[\Omega_i^e\right]^{\Delta\mathbf{s}} + \left[\Omega_i^e\right]^{\Delta\boldsymbol{\beta}^{\mathrm{p}}} + \left[\Omega_i^e\right]^{\Delta\mathbf{s}\Delta\boldsymbol{\beta}^{\mathrm{p}}}$$

with

- $\left[\Omega_i^e\right]^{\Delta\mathbf{s}} = \left[\Omega_i^e\right]\left(\left[\boldsymbol{\beta}^{\mathrm{p}}\right] = 0\right)$, term due to elastic incompatibilities alone $\left(\Delta\mathbf{s}\right)$,
- $\left[\Omega_i^e\right]^{\Delta\boldsymbol{\beta}^{\mathrm{p}}} = \left[\Omega_i^e\right]\left(\left[\Delta\mathbf{s}\right] = 0\right)$, term due to plastic incompatibilities alone ($\Delta\boldsymbol{\beta}^{\mathrm{p}}$),
- $\left[\Omega_i^e\right]^{\Delta\mathbf{s}\Delta\boldsymbol{\beta}^{\mathrm{p}}} = \left[\Omega_i^e\right] - \left(\left[\Omega_i^e\right]^{\Delta\mathbf{s}} + \left[\Omega_i^e\right]^{\Delta\boldsymbol{\beta}^{\mathrm{p}}}\right)$, term due to elastic-plastic coupling incompatibilities $\left(\Delta\mathbf{s}\Delta\boldsymbol{\beta}^{\mathrm{p}}\right)$.

We can notice in Eq.(60) that only $\left[\Omega_1^e\right]$ and $\left[\Omega_3^e\right]$ depend on the three sources of incompatibilities. $\left[\Omega_2^e\right]$ is independent of elastic constants and results only from plastic incompatibilities (see in Appendix C the full expressions of the spin vector jump decomposition).

It is interesting to relate Eq.(60) to the well-known relation established by Kröner (1981) which expresses the gradient of elastic rotation vector in function of elastic strains and Nye's tensor $\boldsymbol{\alpha}$

(63)
$$\mathbf{grad}\,\boldsymbol{\Omega}^{\mathrm{e}} = \left(\mathbf{curl}\,\boldsymbol{\varepsilon}^{\mathrm{e}}\right)^{\mathrm{T}} - \boldsymbol{\alpha}^{\mathrm{T}} + \frac{1}{2}\mathrm{tr}\left(\boldsymbol{\alpha}\right)\mathbf{I}$$

where $\mathbf{I}$ is the unit tensor. Indeed, this equation is expressed in the bulk but in the limit of a vanishing thin planar interface of discontinuity with unit normal $\mathbf{n}$, it becomes (see the proof of this argument in Appendix D)

(64)
$$\left[\boldsymbol{\Omega}^{\mathbf{e}}\right] \otimes \mathbf{n} = -\left(\left[\boldsymbol{\varepsilon}^{\mathrm{e}}\right] \times \mathbf{n}\right)^{\mathrm{T}} - \left(\boldsymbol{\alpha}^{\mathrm{S}}\right)^{\mathrm{T}} + \frac{1}{2}\mathrm{tr}\left(\boldsymbol{\alpha}^{\mathrm{S}}\right)\mathbf{I}$$

The result of Eq.(60) is then exactly retrieved from Eq.(64) when the former is applied to the configuration of Fig.2 (the expression of $\boldsymbol{\alpha}^S$ being given in Eq.(25)).

4.1.1.3 Heterogeneous isotropic elasticity

In the case of heterogeneous isotropic elasticity, many compliance tensor components vanish

$$\begin{cases} \left[\Omega_1^e\right] = \frac{1}{2}\left[\frac{1}{\mu}\right]\Sigma_{23} + \left[\beta_{23}^p\right] \\ \left[\Omega_2^e\right] = \frac{1}{2}\left(\left[\beta_{31}^p\right] - \left[\beta_{13}^p\right]\right) \\ \left[\Omega_3^e\right] = -\left(\frac{1}{2}\left[\frac{1}{\mu}\right]\Sigma_{12} + \left[\beta_{21}^p\right]\right) \end{cases} \tag{65}$$

and the solutions do not depend anymore on coupling incompatibilities.

4.1.1.3 Homogeneous isotropic elasticity

In the case of homogeneous isotropic elasticity, Eq.(60) further simplifies into

$$\begin{cases} \left[\Omega_1^e\right] = \left[\beta_{23}^p\right] \\ \left[\Omega_2^e\right] = \frac{1}{2}\left(\left[\beta_{31}^p\right] - \left[\beta_{13}^p\right]\right) \\ \left[\Omega_3^e\right] = -\left[\beta_{21}^p\right] \end{cases} \tag{66}$$

All the components are then independent of elastic constants.

4.2. Consequence of plastic distortion tangential continuity

If the tangential continuity of the plastic distortion, as described in Section 3.3 (Eq.(20)), is assumed to be satisfied at the interface of Fig.2, we have

$$\left[\beta_{11}^p\right] = \left[\beta_{21}^p\right] = \left[\beta_{31}^p\right] = \left[\beta_{13}^p\right] = \left[\beta_{23}^p\right] = \left[\beta_{33}^p\right] = 0 \tag{67}$$

In the case of piecewise uniform plastic distortions, it conducts to

$$\begin{cases} \sigma_{ij} = \Sigma_{ij} + \sigma_{ij}^{\Delta \mathbf{s}} \\ \left[\Omega_i^e\right] = \left[\Omega_i^e\right]^{\Delta \mathbf{s}} \end{cases} \tag{68}$$

which means that jump of internal stresses and lattice misorientations should be related to elastic incompatibilities only. As a consequence, stresses and lattice misorientations should only develop in an elastic way and thus should recover to zero when the macroscopic uniform stress $\boldsymbol{\Sigma}$ is unloaded to zero (no residual stress and no residual lattice misorientation). In addition we should have in particular $\left[\Omega_2^e\right] = 0$.

In homogeneous elasticity, the tangential continuity of the plastic distortion leads to

$$\begin{cases} \sigma_{ij} = \Sigma_{ij} \\ \left[\Omega_i^e\right] = 0 \end{cases} \tag{69}$$

Hence, it introduces the continuity of both stresses and lattice rotations. Mach et al. (2010) already showed that the tangential jump condition of Eq.(20) can lead to the continuity of

lattice rotations but in the case of a pure viscoplasticity. This result is indeed retrieved from Eqs.(60) and (67) if jumps of elastic strains are neglected. In their paper, Mach et al. (2010) noticed also that in the presence of elastic strains, rotations are no more continuous. Concerning the prediction of texture evolution, it thus appears that an assumption of homogeneous elasticity may actually be equivalent to the hypothesis of a pure viscoplasticity (also true without considering the tangential continuity of the plastic distortion, cf. Eq.(66) and Eq.(60) without elastic strains).

Finally, it should be recalled here that Eqs.(68) and (69) were established in the peculiar case of piecewise uniform plastic distortions. Hence, the tangential continuity of the plastic distortion actually induces the tangential uniformity of plastic distortions, which further leads to a development of stresses and lattice misorientations due only to elastic heterogeneous properties. In the more realistic case of tangentially continuous but not necessarily uniform plastic distortions (which is not the scope of the present paper), stress and lattice misorientation evolutions should be very much related to the limiting values of the tangential plastic distortions at the interface as seen for instance from numerical simulations in Richeton et al. (2011) and Taupin et al. (2012).

5. Application to bicrystals deformation

The first part of this section aims at checking the correctness of the analytical formulas established in Section 4 from Crystal Plasticity Finite Element simulations and then at showing the relative contribution of the different sources of incompatibilities. The second part of the section deals with elastic/plastic bicrystals and displays the values of residual stresses and residual lattice misorientations for different orientations of the elastic crystal. Systematic comparisons with the isotropic approximations are also performed.

5.1. Finite element modelling of a bicrystal with infinite planar interface

5.1.1 Description of the crystal plasticity model

A 3D finite element mesh of 20-node brick elements with reduced integration (C3D20R) is used for the discretization a bicrystal bar (10 x 100 x 10 elements, see Fig.3). This bicrystal bar is designed to mimic the configuration of Fig.2. Periodic boundary conditions are indeed imposed along the lateral sides. The two crystals are thus separated by an infinite planar interface with normal along (O,x_2) (Fig.3). Fixed velocities are prescribed on the upper and bottom face (Fig.3). Besides, a simplified single crystal plasticity model inspired by the work of Peirce et al. (1983) is implemented at small strains within a Finite Element commercial software (ABAQUS/Standard). For the sake of further analyses'clarity, our model assumes that plasticity results solely from the possible activation of a single slip system (hence, there is no consideration of latent hardening). The plastic velocity gradient tensor $\mathbf{L}^p$ is then conventionally expressed as

$$\mathbf{L}_p = \dot{\gamma}\ \mathbf{s} \otimes \mathbf{m} \tag{70}$$

where $\mathbf{s}$ and $\mathbf{m}$ are the slip direction vector and glide plane normal, respectively. The plastic slip rate on the single slip system $\dot{\gamma}$ is given by the Orowan's law, $\dot{\gamma} = \rho_m b V_d$. ρ_m is the density of mobile dislocations, which is here assumed to remain constant. b is the magnitude of the Burgers vector and V_d is the averaged collective dislocation velocity on the slip system. V_d is assumed to follow the power law relationship

$$V_d = V_0\ \mathrm{sgn}(\tau)\left(\frac{|\tau|}{\sigma_h}\right)^n \tag{71}$$

where $\tau = \mathbf{s} \otimes \mathbf{m} : \boldsymbol{\sigma}$ is the resolved shear stress on the glide plane, with reference velocity V_0 and stress exponent *n* as material parameters. $\mathrm{sgn}(\tau) = 1$ when $\tau > 0$ and $\mathrm{sgn}(\tau) = -1$ when $\tau < 0$. The reference shear stress σ_h reflects short range obstacle overcoming for dislocations. In this simplified model, the reference shear stress is allocated a stationary value, meaning that no isotropic hardening is considered. The implementation of this model is made through the use of the rate tangent modulus method developed by Peirce et al. (1984). A linear interpolation within the time increment Δt is thus employed to define the increment of plastic shear strain $\Delta\gamma$

$$\Delta\gamma = \Delta t\left[(1-\chi)\dot{\gamma}_t + \chi\dot{\gamma}_{t+\Delta t}\right] \tag{72}$$

where the time integration parameter χ ranges from 0 to 1 with $\chi = 0$ corresponding to the Euler forward explicit integration scheme. Here, a classical value of 0.5 is chosen (see Peirce et al., 1984).

Cubic symmetry elastic stiffnesses for copper are given in Table 1 and are considered to run the simulation. Other material parameters are given in Table 2. On the upper and bottom face, the following material velocities are prescribed

$$\mathrm{v}_2 = \pm L\dot{\Gamma} \text{ and } \mathrm{v}_1 = \mathrm{v}_3 = 0 \text{ along } x_2 = \pm L \tag{73}$$

where $\dot{\Gamma} = 10^{-3}\ \mathrm{s}^{-1}$ is the initial applied macroscopic strain rate and $L = 50\ \mu\mathrm{m}$ is the initial length along (O,x_2) of each crystal. It should be noted that this loading test does not correspond to a pure tensile test since all the components of the macroscopic stress tensor are non zero. Indeed, constraining the cross-sectional contraction of the material by prescribing zero transverse velocities at the sample ends ($\mathrm{v}_1 = \mathrm{v}_3 = 0$) leads to transverse reaction forces. The component Σ_{22} remains however the prevailing one close to a pure uniaxial tensile load. The crystals orientations are indicated in Table 2. Crystal I has the crystallographic direction $[123]$ along the tensile axis, which corresponds to a typical single slip orientation for a fcc single crystal (Takeuchi, 1975), therefore justifying our model's simplifying assumption (Eq.(70)). Plasticity in crystal I thus solely results from dislocation glide on the system $\langle 101\rangle\left[\bar{1}11\right]$. The threshold shear stress σ_h is affected by a very huge value in crystal II, so that the behavior of crystal II remains purely elastic during the small range of tensile strains (< 0.2 %) investigated in the FE simulation. This consideration is justified by the chosen orientation for crystal II (Table 2). In the elastic domain, crystal II exhibits much lower resolved shear stresses on its slip systems than the shear stress on system $\langle 101\rangle\left[\bar{1}11\right]$ in crystal I. As a consequence, crystal II should normally be in a plastic state much later on than crystal I.

5.1.2 Validation of the explicit closed-from solutions

The infinite planar interface under study thus separates a crystal undergoing elasticity and single slip plasticity from a crystal of the same composition but with a different orientation and which undergoes only elasticity. Fig.4 exhibits a comparison between the stresses in crystal II provided by the FE simulation (σ_{ij}^{num}) and those directly derived from the expressions of Eq.(45) (σ_{ij}^{theo}). It is noteworthy that the former formulas are static whereas the FE calculations are a consequence of an incremental procedure based on an evolving viscoplastic strain as defined in Eqs.(70) to (72). σ_{ij}^{theo} is actually computed from

Eq.(45) with the overall stress $\boldsymbol{\Sigma}$ and the jumps of plastic strain jump $\left[\boldsymbol{\varepsilon}^{\mathrm{p}}\right]$ taken from the FE calculations and updated after each time increment. In the same way, Fig.5 shows a comparison between the lattice misorientations provided by the FE simulation ($\left[\boldsymbol{\Omega}_i^{\mathrm{e}}\right]^{num}$) and those directly derived from the analytical formulas ($\left[\boldsymbol{\Omega}_i^{\mathrm{e}}\right]^{theo}$ computed from Eq.(60) with $\boldsymbol{\Sigma}$ and the jump of plastic distortions $\left[\boldsymbol{\beta}^{\mathrm{p}}\right]$ as inputs). For both cases, it can be seen that the FE solutions match perfectly the analytical ones (the differences being within the numerical precision of the computer) thus giving a proof of the correctness of the formulas established in Section 4.

5.1.3 Relative contribution of the different sources of incompatibilities

From the evolution of $\boldsymbol{\Sigma}$ and $\left[\boldsymbol{\beta}^{\mathrm{p}}\right]$ provided by the FE simulation, our analytical developments enable to quantify the contribution of the different incompatibility sources on stresses and lattice misorientations as exposed in Eqs.(46) and (62). Examples of these decompositions are given in crystal II for σ_{11} and $\left[\Omega_1^e\right]$ in Figs. 6 and 7, taking the plastic crystal (crystal I) as the reference medium. For the present elastic/plastic bicrystal, the major contribution arises from the terms due to plastic incompatibilities alone ($\sigma_{ij}^{\Delta\boldsymbol{\varepsilon}^{\mathrm{p}}}$, $\left[\Omega_i^e\right]^{\Delta\boldsymbol{\beta}^{\mathrm{p}}}$). However, it can be observed that the other terms ($\sigma_{ij}^{\Delta\mathbf{s}}$, $\sigma_{ij}^{\Delta\mathbf{s}\Delta\boldsymbol{\varepsilon}^{\mathrm{p}}}$, $\left[\Omega_i^e\right]^{\Delta\mathbf{s}}$, $\left[\Omega_i^e\right]^{\Delta\mathbf{s}\Delta\boldsymbol{\beta}^{\mathrm{p}}}$), which would be absent in homogeneous elasticity, still represent a significant part. It can notably be inferred that the coupling term between elastic and plastic incompatibilities might exhibit huge contributions for some peculiar configurations. For instance, in Fig.7, contribution of coupling incompatibilities on $\left[\Omega_1^e\right]$ is quite consequent and opposite in sign with respect to the one due to plastic incompatibilities alone. Therefore, heterogeneous elasticity may influence strongly on texture developments in the course of plastic deformation in polycrystalline aggregates. This aspect is often neglected in the crystallographic texture developments simulated by polycrystalline models (Self-Consistent models, Crystal Plasticity Finite Element models or FDM models restricted to pure viscoplastic behaviour or elastic-viscoplastic behaviour with homogeneous isotropic elasticity).

5.2. Analytical predictions of residual stresses and lattice misorientations

The same bicrystal than in Section 5.1 is used as a starting configuration. While the plastic crystal (crystal I) remains fixed, the elastic one (crystal II) is subsequently authorized to rotate around (O,x_2) by an angle θ. Indeed, in case of a tensile test, the resolved shear stresses on slip systems remain unchanged when the crystal is rotated around the tensile axis. It can thus be assumed that crystal II undergoes pure elastic distortions for any value of θ, providing that the tensile strain remains low enough. Then, assuming a given low value of plastic slip (results are shown for $\gamma = 0.01$) for the system $\langle 101\rangle\left[\bar{1}11\right]$ in crystal I, the analytical formulas of Section 4 enable to derive directly the residual stresses and the residual lattice misorientations of the elastic/plastic bicrystal (i.e. Eqs.(45) and (60) are used with $\boldsymbol{\Sigma} = 0$, i.e. $\left[\varepsilon_{11}^*\right] = \left[\varepsilon_{11}^p\right]$, $\left[\varepsilon_{33}^*\right] = \left[\varepsilon_{33}^p\right]$, $\left[\varepsilon_{31}^*\right] = \left[\varepsilon_{31}^p\right]$ in Eq.(44)). In the case $\boldsymbol{\Sigma} = 0$, we have precisely

(74)
$$\begin{cases} \sigma_{ij} = \sigma_{ij}^{\Delta\boldsymbol{\varepsilon}^{\mathrm{p}}} + \sigma_{ij}^{\Delta\mathbf{s}\Delta\boldsymbol{\varepsilon}^{\mathrm{p}}} \\ \left[\Omega_i^e\right] = \left[\Omega_i^e\right]^{\Delta\boldsymbol{\beta}^{\mathrm{p}}} + \left[\Omega_i^e\right]^{\Delta\mathbf{s}\Delta\boldsymbol{\beta}^{\mathrm{p}}} \end{cases}$$

Figs. 8, 9 and 10 display respectively the evolution of residual stress components σ_{11}, σ_{33}, σ_{31}, stored elastic energy density φ and residual lattice misorientation vector components $\left[\Omega_1^e\right]$ and $\left[\Omega_3^e\right]$ in function of θ for γ = 0.01. Results derived from the general consideration of heterogeneous anisotropic elasticity are compared with solutions derived from isotropic approximations (the isotropic average elastic constants are computed from a Voigt average (Hirth and Lothe, 1982), see Table 1) which involves the dying out of the coupling terms in Eq.(74). Results are also displayed for two fcc materials, Cu which is strongly anisotropic (anisotropic coefficient $\mathrm{a} = 2c_{44}/\left(c_{11} - c_{12}\right) = 3.26$), and Al which is quite less ($\mathrm{a} = 1.22$, see Table 1). The difference between Cu and Al in stresses and in the density of stored elastic energy (Figs. 8 and 9) arises solely because of different values of elastic coefficients in crystal I. Isotropic assumption leads however to the same solutions for Cu and Al concerning the lattice misorientation vector, since the former do not depend on elastic constants in this case (Eq.(66)). In the general heterogeneous anisotropic case, lattice misorientations do depend on elastic constants, as it is illustrated in Fig.10 where a consequent difference between Cu and Al is observed. In the same way, concerning stresses and stored elastic energy density, Figs. 8 and 9 show that the discrepancy between isotropic and anisotropic solutions is much more pronounced for Cu than for Al. From the insets of Figs. 8, 9 and 10, it is seen that the relative error made by the isotropic approximation is strongly dependent on the orientation of crystal II and can reach values above 40% in Cu. Strong discrepancies can occur for both stresses and lattice misorientations. For 1% slip, the rotation of the elastic crystal around the tensile axis can lead in Cu to a stress variation reaching 50 MPa (Fig.8) and a lattice rotation variation reaching 0.1° (Fig.10).

As a consequence, considering elastic anisotropy is crucial not only to predict stresses with good accuracy but also to predict correct texture evolution. Besides, several crystals may display higher elastic anisotropy than pure Cu (e.g., $\mathrm{a} = 8.91$ for β-brass or $\mathrm{a} = 12.5$ for a Cu-14wt.% Al-4.2wt.% Ni alloy, see Suezawa and Sumini, 1976). This study also illustrates the role that elastic anisotropy may have on strain path dependence in polycrystals. In the course of a Bauschinger test for instance, fields due to pure elastic incompatibilities will recover to zero when $\boldsymbol{\Sigma} = 0$ (Yaguchi and Margolin, 1986) but fields due to elastic-plastic coupling incompatibilities will remain in addition to fields due to pure plastic incompatibilities. It must be noted that elastic incompatibilities may nevertheless influence the Bauschinger effect by contributing to the selection of slip systems and affecting their activity around the grain boundary (Vehoff et al., 1987; Yaguchi and Margolin, 1986). Furthermore, in fatigue tests, elastic incompatibilities alone can induce some plasticity near the grain boundary (Vehoff et al., 1987; Yaguchi and Margolin, 1986). As a result of cumulative plastic strain, plastic and coupling incompatibilities also develop and provoke stress concentrations which may finally lead to crack initiation.

6. Conclusions

The present paper considered the issue of bicrystal elasto-plasticity assuming an infinite planar grain boundary. The bicrystal is considered as a heterogeneous elastic-plastic solid undergoing piecewise uniform plastic distortions (where plasticity is not restricted to be incompressible) and elastic properties. Explicit closed-form solutions of

stress and lattice misorientation fields in the general context of heterogeneous anisotropic elasticity (with and without plastic distortion tangential continuity) were derived by use of the concepts of Field Dislocation Mechanics in the context of Frank-Bilby interfacial dislocation. The obtained expressions were validated by Crystal Plasticity Finite Element simulations on a bicrystal with periodic boundary conditions. Analytical solutions made it possible to quantify the contributions of the different incompatibility sources, namely the contribution arising from elastic incompatibilities alone, that due to plastic incompatibilities alone and the one due couplings between elastic and plastic incompatibilities. Applications were performed on infinite elastic/plastic bicrystals for different orientations of the elastic crystal. Values of residual stresses and lattice misorientations were compared with the isotropic approximations. In most situations, plastic incompatibilities had the most prominent effects but elastic and even more coupling incompatibilities showed significant contributions depending on the material elastic constants, the relative orientation of both crystals and the external loading. However, it must be recalled here that the study was conducted in single slip plasticity only as it was restricted to small value of plastic slip. With increasing plastic slip, allowing for multiple slip systems activity and latent hardening will strongly affect the evolution of $\boldsymbol{\Sigma}$ and $\left[\boldsymbol{\beta}^{p}\right]$. The validity of the obtained analytical expressions will still remain under the assumptions considered (i.e. linear anisotropic elasticity and homogeneous plastic distortion within each crystal) but the relative part of the different incompatibility terms of $\boldsymbol{\sigma}$ and $\left[\boldsymbol{\Omega}^{e}\right]$ may evolve differently from the results exposed in Figs.6 and 7. In the same way, plastic accommodation on different slip systems could modify the discrepancy between the anisotropic solutions and the isotropic approximations (Figs.8, 9, 10) with increasing plastic slip.

Only plastic and elastic-plastic coupling incompatibilities do contribute directly to residual fields. Under load however, all incompatibility types may affect the selection of slip systems and therefore the distribution of plastic strains. Because of elastic-plastic coupling incompatibilities, the necessity to consider elastic anisotropy in models for accurate prediction of residual textures is also demonstrated. Actually, it has been shown in the present paper that an assumption of homogeneous elasticity restricts to the hypothesis of pure viscoplasticity. Finally, as discussed by Gemperlova et al. (1989), it must be underlined that the expressions of stresses and lattice misorientations obtained in an infinite bicrystal should be valid in a finite bicrystal only in a thin region adjacent to the interface and far from the finite boundaries and edges like free surfaces. In polycrystalline aggregates, these field expressions might give some correct estimates close to grain boundaries and far from triple junctions. In addition, it should be mentioned that they remain valid if the interface considered is a twin or a phase boundary. Therefore, the derived formulas are expected to be also of some use in dealing with twinning or multiphase alloys deformation and fatigue issues.

Acknowledgements
TR is grateful to the French Agence nationale de la Recherche (ANR) for financial support under contract “PHIRCILE” (ANR 2010 JCJC 0914 01).

Appendix A. Development of the compatibility conditions

The full development of the compatibility conditions ($\operatorname{curl}\boldsymbol{\beta}^{e}_{\square} = \operatorname{curl}\boldsymbol{\beta}^{p}_{\square} = 0$, Eq.(3)c) writes

(A.1)
$$\begin{pmatrix} \beta^{e}_{\square 13,2}-\beta^{e}_{\square 12,3} & \beta^{e}_{\square 11,3}-\beta^{e}_{\square 13,1} & \beta^{e}_{\square 12,1}-\beta^{e}_{\square 11,2} \\ \beta^{e}_{\square 23,2}-\beta^{e}_{\square 22,3} & \beta^{e}_{\square 21,3}-\beta^{e}_{\square 23,1} & \beta^{e}_{\square 22,1}-\beta^{e}_{\square 21,2} \\ \beta^{e}_{\square 33,2}-\beta^{e}_{\square 32,3} & \beta^{e}_{\square 31,3}-\beta^{e}_{\square 33,1} & \beta^{e}_{\square 32,1}-\beta^{e}_{\square 31,2} \end{pmatrix}$$
$$= \begin{pmatrix} \beta^{p}_{\square 13,2}-\beta^{p}_{\square 12,3} & \beta^{p}_{\square 11,3}-\beta^{p}_{\square 13,1} & \beta^{p}_{\square 12,1}-\beta^{p}_{\square 11,2} \\ \beta^{p}_{\square 23,2}-\beta^{p}_{\square 22,3} & \beta^{p}_{\square 21,3}-\beta^{p}_{\square 23,1} & \beta^{p}_{\square 22,1}-\beta^{p}_{\square 21,2} \\ \beta^{p}_{\square 33,2}-\beta^{p}_{\square 32,3} & \beta^{p}_{\square 31,3}-\beta^{p}_{\square 33,1} & \beta^{p}_{\square 32,1}-\beta^{p}_{\square 31,2} \end{pmatrix} = \begin{pmatrix} 0 & 0 & 0 \\ 0 & 0 & 0 \\ 0 & 0 & 0 \end{pmatrix}$$

Appendix B. Full explicit component expressions of the elastic concentration and influence tensors obtained from Eq.(45)

Following Eq.(45), the elastic stress concentration tensor components of $B^{\square\square}_{PP'}$ present in Eq.(53) are first formulated (with the same notations as in the main text)

(B.1)
$$\begin{cases} B^{\square\square}_{1111} = -\dfrac{2\left[s^{\square}_{11}\left(\tilde{s}_{33}\tilde{s}_{55}-\tilde{s}_{35}{}^{2}\right)+s^{\square}_{13}\left(\tilde{s}_{15}\tilde{s}_{35}-\tilde{s}_{13}\tilde{s}_{55}\right)+s^{\square}_{15}\left(\tilde{s}_{13}\tilde{s}_{35}-\tilde{s}_{33}\tilde{s}_{15}\right)\right]}{D} \\ B^{\square\square}_{1133} = -\dfrac{2\left[s^{\square}_{13}\left(\tilde{s}_{33}\tilde{s}_{55}-\tilde{s}_{35}{}^{2}\right)+s^{\square}_{33}\left(\tilde{s}_{15}\tilde{s}_{35}-\tilde{s}_{13}\tilde{s}_{55}\right)+s^{\square}_{35}\left(\tilde{s}_{13}\tilde{s}_{35}-\tilde{s}_{33}\tilde{s}_{15}\right)\right]}{D} \\ B^{\square\square}_{1113} = B^{\square\square}_{1131} = -\dfrac{2\left[s^{\square}_{15}\left(\tilde{s}_{33}\tilde{s}_{55}-\tilde{s}_{35}{}^{2}\right)+s^{\square}_{35}\left(\tilde{s}_{15}\tilde{s}_{35}-\tilde{s}_{13}\tilde{s}_{55}\right)+s^{\square}_{55}\left(\tilde{s}_{13}\tilde{s}_{35}-\tilde{s}_{33}\tilde{s}_{15}\right)\right]}{D} \\ B^{\square\square}_{3311} = -\dfrac{2\left[s^{\square}_{11}\left(\tilde{s}_{15}\tilde{s}_{35}-\tilde{s}_{13}\tilde{s}_{55}\right)+s^{\square}_{13}\left(\tilde{s}_{11}\tilde{s}_{55}-\tilde{s}_{15}{}^{2}\right)+s^{\square}_{15}\left(\tilde{s}_{13}\tilde{s}_{15}-\tilde{s}_{11}\tilde{s}_{35}\right)\right]}{D} \\ B^{\square\square}_{3333} = -\dfrac{2\left[s^{\square}_{13}\left(\tilde{s}_{15}\tilde{s}_{35}-\tilde{s}_{13}\tilde{s}_{55}\right)+s^{\square}_{33}\left(\tilde{s}_{11}\tilde{s}_{55}-\tilde{s}_{15}{}^{2}\right)+s^{\square}_{35}\left(\tilde{s}_{13}\tilde{s}_{15}-\tilde{s}_{11}\tilde{s}_{35}\right)\right]}{D} \\ B^{\square\square}_{3313} = B^{\square\square}_{3331} = -\dfrac{2\left[s^{\square}_{15}\left(\tilde{s}_{15}\tilde{s}_{35}-\tilde{s}_{13}\tilde{s}_{55}\right)+s^{\square}_{35}\left(\tilde{s}_{11}\tilde{s}_{55}-\tilde{s}_{15}{}^{2}\right)+s^{\square}_{55}\left(\tilde{s}_{13}\tilde{s}_{15}-\tilde{s}_{11}\tilde{s}_{35}\right)\right]}{D} \\ B^{\square\square}_{1311} = B^{\square\square}_{3111} = -\dfrac{2\left[s^{\square}_{11}\left(\tilde{s}_{13}\tilde{s}_{35}-\tilde{s}_{33}\tilde{s}_{15}\right)+s^{\square}_{13}\left(\tilde{s}_{13}\tilde{s}_{15}-\tilde{s}_{11}\tilde{s}_{35}\right)+s^{\square}_{15}\left(\tilde{s}_{11}\tilde{s}_{33}-\tilde{s}_{13}{}^{2}\right)\right]}{D} \\ B^{\square\square}_{1333} = B^{\square\square}_{3133} = -\dfrac{2\left[s^{\square}_{13}\left(\tilde{s}_{13}\tilde{s}_{35}-\tilde{s}_{33}\tilde{s}_{15}\right)+s^{\square}_{33}\left(\tilde{s}_{13}\tilde{s}_{15}-\tilde{s}_{11}\tilde{s}_{35}\right)+s^{\square}_{35}\left(\tilde{s}_{11}\tilde{s}_{33}-\tilde{s}_{13}{}^{2}\right)\right]}{D} \\ B^{\square\square}_{1313} = B^{\square\square}_{1331} = B^{\square\square}_{3113} = B^{\square\square}_{3131} = -\dfrac{2\left[s^{\square}_{15}\left(\tilde{s}_{13}\tilde{s}_{35}-\tilde{s}_{33}\tilde{s}_{15}\right)+s^{\square}_{35}\left(\tilde{s}_{13}\tilde{s}_{15}-\tilde{s}_{11}\tilde{s}_{35}\right)+s^{\square}_{55}\left(\tilde{s}_{11}\tilde{s}_{33}-\tilde{s}_{13}{}^{2}\right)\right]}{D} \end{cases}$$

where $D = \tilde{s}_{11}\tilde{s}_{35}{}^2 + \tilde{s}_{33}\tilde{s}_{15}{}^2 + \tilde{s}_{55}\tilde{s}_{13}{}^2 - \tilde{s}_{11}\tilde{s}_{33}\tilde{s}_{55} - 2\tilde{s}_{13}\tilde{s}_{15}\tilde{s}_{35}$ is the common denominator term in Eq.(45).

From Eq.(45), the elastic stress concentration tensor components of B^{II}_{PA} present in Eq.(53) are given by

$$
\begin{cases}
B^{II}_{1122} = \dfrac{[s_{12}]\left(\tilde{s}_{33}\tilde{s}_{55} - \tilde{s}_{35}{}^2\right) + [s_{23}]\left(\tilde{s}_{15}\tilde{s}_{35} - \tilde{s}_{13}\tilde{s}_{55}\right) + [s_{25}]\left(\tilde{s}_{13}\tilde{s}_{35} - \tilde{s}_{33}\tilde{s}_{15}\right)}{D} \\
B^{II}_{1112} = B^{II}_{1121} = \dfrac{[s_{14}]\left(\tilde{s}_{33}\tilde{s}_{55} - \tilde{s}_{35}{}^2\right) + [s_{34}]\left(\tilde{s}_{15}\tilde{s}_{35} - \tilde{s}_{13}\tilde{s}_{55}\right) + [s_{45}]\left(\tilde{s}_{13}\tilde{s}_{35} - \tilde{s}_{33}\tilde{s}_{15}\right)}{D} \\
B^{II}_{1123} = B^{II}_{1132} = \dfrac{[s_{16}]\left(\tilde{s}_{33}\tilde{s}_{55} - \tilde{s}_{35}{}^2\right) + [s_{36}]\left(\tilde{s}_{15}\tilde{s}_{35} - \tilde{s}_{13}\tilde{s}_{55}\right) + [s_{56}]\left(\tilde{s}_{13}\tilde{s}_{35} - \tilde{s}_{33}\tilde{s}_{15}\right)}{D} \\
B^{II}_{3322} = \dfrac{[s_{12}]\left(\tilde{s}_{15}\tilde{s}_{35} - \tilde{s}_{13}\tilde{s}_{55}\right) + [s_{23}]\left(\tilde{s}_{11}\tilde{s}_{55} - \tilde{s}_{15}{}^2\right) + [s_{25}]\left(\tilde{s}_{13}\tilde{s}_{15} - \tilde{s}_{11}\tilde{s}_{35}\right)}{D} \\
B^{II}_{3312} = B^{II}_{3321} = \dfrac{[s_{14}]\left(\tilde{s}_{15}\tilde{s}_{35} - \tilde{s}_{13}\tilde{s}_{55}\right) + [s_{34}]\left(\tilde{s}_{11}\tilde{s}_{55} - \tilde{s}_{15}{}^2\right) + [s_{45}]\left(\tilde{s}_{13}\tilde{s}_{15} - \tilde{s}_{11}\tilde{s}_{35}\right)}{D} \\
B^{II}_{3323} = B^{II}_{3332} = \dfrac{[s_{16}]\left(\tilde{s}_{15}\tilde{s}_{35} - \tilde{s}_{13}\tilde{s}_{55}\right) + [s_{36}]\left(\tilde{s}_{11}\tilde{s}_{55} - \tilde{s}_{15}{}^2\right) + [s_{56}]\left(\tilde{s}_{13}\tilde{s}_{15} - \tilde{s}_{11}\tilde{s}_{35}\right)}{D} \\
B^{II}_{1322} = B^{II}_{3122} = \dfrac{[s_{12}]\left(\tilde{s}_{13}\tilde{s}_{35} - \tilde{s}_{33}\tilde{s}_{15}\right) + [s_{23}]\left(\tilde{s}_{13}\tilde{s}_{15} - \tilde{s}_{11}\tilde{s}_{35}\right) + [s_{25}]\left(\tilde{s}_{11}\tilde{s}_{33} - \tilde{s}_{13}{}^2\right)}{D} \\
B^{II}_{1312} = B^{II}_{1321} = B^{II}_{3112} = B^{II}_{3121} = \dfrac{[s_{14}]\left(\tilde{s}_{13}\tilde{s}_{35} - \tilde{s}_{33}\tilde{s}_{15}\right) + [s_{34}]\left(\tilde{s}_{13}\tilde{s}_{15} - \tilde{s}_{11}\tilde{s}_{35}\right) + [s_{45}]\left(\tilde{s}_{11}\tilde{s}_{33} - \tilde{s}_{13}{}^2\right)}{D} \\
B^{II}_{1323} = B^{II}_{1332} = B^{II}_{3123} = B^{II}_{3132} = \dfrac{[s_{16}]\left(\tilde{s}_{13}\tilde{s}_{35} - \tilde{s}_{33}\tilde{s}_{15}\right) + [s_{36}]\left(\tilde{s}_{13}\tilde{s}_{15} - \tilde{s}_{11}\tilde{s}_{35}\right) + [s_{56}]\left(\tilde{s}_{11}\tilde{s}_{33} - \tilde{s}_{13}{}^2\right)}{D}
\end{cases}
\tag{B.2}
$$

Lastly, from Eq.(45), the non zero stress influence tensor components $F_{PP'}$ in Eq.(53) yield

(B.3)
$$\begin{cases} \mathrm{F}_{1111} = \dfrac{\tilde{s}_{33}\tilde{s}_{55} - \tilde{s}_{35}^{\,2}}{D} \\ \mathrm{F}_{3333} = \dfrac{\tilde{s}_{11}\tilde{s}_{55} - \tilde{s}_{15}^{\,2}}{D} \\ \mathrm{F}_{1313} = \mathrm{F}_{3113} = \mathrm{F}_{1331} = \mathrm{F}_{3131} = \dfrac{\tilde{s}_{11}\tilde{s}_{33} - \tilde{s}_{13}^{\,2}}{D} \\ \mathrm{F}_{1133} = \mathrm{F}_{3311} = \dfrac{\tilde{s}_{15}\tilde{s}_{35} - \tilde{s}_{13}\tilde{s}_{55}}{D} \\ \mathrm{F}_{1113} = \mathrm{F}_{1131} = \mathrm{F}_{1311} = \mathrm{F}_{3111} = \dfrac{\tilde{s}_{13}\tilde{s}_{35} - \tilde{s}_{33}\tilde{s}_{15}}{D} \\ \mathrm{F}_{3313} = \mathrm{F}_{3331} = \mathrm{F}_{1333} = \mathrm{F}_{3133} = \dfrac{\tilde{s}_{13}\tilde{s}_{15} - \tilde{s}_{11}\tilde{s}_{35}}{D} \end{cases}$$

Appendix C. Full explicit expressions of the spin vector jump decomposition

(C.1)
$$\begin{cases} \left[\Omega_1^e\right]^{\Delta\mathbf{s}} = s_{16}^{\boxed{\mathrm{I}}}\sigma_{11}^{\boxed{\mathrm{II}}\Delta\mathbf{s}} + s_{36}^{\boxed{\mathrm{I}}}\sigma_{33}^{\boxed{\mathrm{II}}\Delta\mathbf{s}} + s_{46}^{\boxed{\mathrm{I}}}\sigma_{31}^{\boxed{\mathrm{II}}\Delta\mathbf{s}} \\ +\dfrac{1}{2}\left(\left[s_{16}\right]\left(\Sigma_{11} + \sigma_{11}^{\boxed{\mathrm{II}}\Delta\mathbf{s}}\right) + \left[s_{36}\right]\left(\Sigma_{33} + \sigma_{33}^{\boxed{\mathrm{II}}\Delta\mathbf{s}}\right) + \left[s_{56}\right]\left(\Sigma_{31} + \sigma_{31}^{\boxed{\mathrm{II}}\Delta\mathbf{s}}\right) + \left[s_{26}\right]\Sigma_{22} + \left[s_{46}\right]\Sigma_{12} + \left[s_{66}\right]\Sigma_{23}\right) \\ \left[\Omega_2^e\right]^{\Delta\mathbf{s}} = 0 \\ \left[\Omega_3^e\right]^{\Delta\mathbf{s}} = -\left(s_{14}^{\boxed{\mathrm{I}}}\sigma_{11}^{\boxed{\mathrm{II}}\Delta\mathbf{s}} + s_{34}^{\boxed{\mathrm{I}}}\sigma_{33}^{\boxed{\mathrm{II}}\Delta\mathbf{s}} + s_{45}^{\boxed{\mathrm{I}}}\sigma_{31}^{\boxed{\mathrm{II}}\Delta\mathbf{s}}\right) \\ -\dfrac{1}{2}\left(\left[s_{14}\right]\left(\Sigma_{11} + \sigma_{11}^{\boxed{\mathrm{II}}\Delta\mathbf{s}}\right) + \left[s_{34}\right]\left(\Sigma_{33} + \sigma_{33}^{\boxed{\mathrm{II}}\Delta\mathbf{s}}\right) + \left[s_{45}\right]\left(\Sigma_{31} + \sigma_{31}^{\boxed{\mathrm{II}}\Delta\mathbf{s}}\right) + \left[s_{24}\right]\Sigma_{22} + \left[s_{44}\right]\Sigma_{12} + \left[s_{46}\right]\Sigma_{23}\right) \end{cases}$$

(C.2)
$$\begin{cases} \left[\Omega_1^e\right]^{\Delta\boldsymbol{\beta}^{\mathrm{p}}} = s_{16}^{\boxed{\mathrm{I}}}\sigma_{11}^{\boxed{\mathrm{II}}\Delta\boldsymbol{\varepsilon}^{\mathrm{p}}} + s_{36}^{\boxed{\mathrm{I}}}\sigma_{33}^{\boxed{\mathrm{II}}\Delta\boldsymbol{\varepsilon}^{\mathrm{p}}} + s_{46}^{\boxed{\mathrm{I}}}\sigma_{31}^{\boxed{\mathrm{II}}\Delta\boldsymbol{\varepsilon}^{\mathrm{p}}} + \left[\beta_{23}^p\right] \\ \left[\Omega_2^e\right]^{\Delta\boldsymbol{\beta}^{\mathrm{p}}} = \dfrac{1}{2}\left(\left[\beta_{31}^p\right] - \left[\beta_{13}^p\right]\right) \\ \left[\Omega_3^e\right]^{\Delta\boldsymbol{\beta}^{\mathrm{p}}} = -\left(s_{14}^{\boxed{\mathrm{I}}}\sigma_{11}^{\boxed{\mathrm{II}}\Delta\boldsymbol{\varepsilon}^{\mathrm{p}}} + s_{34}^{\boxed{\mathrm{I}}}\sigma_{33}^{\boxed{\mathrm{II}}\Delta\boldsymbol{\varepsilon}^{\mathrm{p}}} + s_{45}^{\boxed{\mathrm{I}}}\sigma_{31}^{\boxed{\mathrm{II}}\Delta\boldsymbol{\varepsilon}^{\mathrm{p}}} + \left[\beta_{21}^p\right]\right) \end{cases}$$

(C.3)
$$\begin{cases} \left[\Omega_1^e\right]^{\Delta\mathbf{s}\Delta\boldsymbol{\beta}^{\mathrm{p}}} = s_{16}^{\boxed{\mathrm{I}}}\sigma_{11}^{\boxed{\mathrm{II}}\Delta\mathbf{s}\Delta\boldsymbol{\varepsilon}^{\mathrm{p}}} + s_{36}^{\boxed{\mathrm{I}}}\sigma_{33}^{\boxed{\mathrm{II}}\Delta\mathbf{s}\Delta\boldsymbol{\varepsilon}^{\mathrm{p}}} + s_{46}^{\boxed{\mathrm{I}}}\sigma_{31}^{\boxed{\mathrm{II}}\Delta\mathbf{s}\Delta\boldsymbol{\varepsilon}^{\mathrm{p}}} \\ +\frac{1}{2}\left(\left[s_{16}\right]\left(\sigma_{11}^{\boxed{\mathrm{II}}\Delta\boldsymbol{\varepsilon}^{\mathrm{p}}} + \sigma_{11}^{\boxed{\mathrm{II}}\Delta\mathbf{s}\Delta\boldsymbol{\varepsilon}^{\mathrm{p}}}\right) + \left[s_{36}\right]\left(\sigma_{33}^{\boxed{\mathrm{II}}\Delta\boldsymbol{\varepsilon}^{\mathrm{p}}} + \sigma_{33}^{\boxed{\mathrm{II}}\Delta\mathbf{s}\Delta\boldsymbol{\varepsilon}^{\mathrm{p}}}\right) + \left[s_{56}\right]\left(\sigma_{31}^{\boxed{\mathrm{II}}\Delta\boldsymbol{\varepsilon}^{\mathrm{p}}} + \sigma_{31}^{\boxed{\mathrm{II}}\Delta\mathbf{s}\Delta\boldsymbol{\varepsilon}^{\mathrm{p}}}\right)\right) \\ \left[\Omega_2^e\right]^{\Delta\mathbf{s}\Delta\boldsymbol{\beta}^{\mathrm{p}}} = 0 \\ \left[\Omega_3^e\right]^{\Delta\mathbf{s}\Delta\boldsymbol{\beta}^{\mathrm{p}}} = -\left(s_{14}^{\boxed{\mathrm{I}}}\sigma_{11}^{\boxed{\mathrm{II}}\Delta\mathbf{s}\Delta\boldsymbol{\varepsilon}^{\mathrm{p}}} + s_{34}^{\boxed{\mathrm{I}}}\sigma_{33}^{\boxed{\mathrm{II}}\Delta\mathbf{s}\Delta\boldsymbol{\varepsilon}^{\mathrm{p}}} + s_{45}^{\boxed{\mathrm{I}}}\sigma_{31}^{\boxed{\mathrm{II}}\Delta\mathbf{s}\Delta\boldsymbol{\varepsilon}^{\mathrm{p}}}\right) \\ -\frac{1}{2}\left(\left[s_{14}\right]\left(\sigma_{11}^{\boxed{\mathrm{II}}\Delta\boldsymbol{\varepsilon}^{\mathrm{p}}} + \sigma_{11}^{\boxed{\mathrm{II}}\Delta\mathbf{s}\Delta\boldsymbol{\varepsilon}^{\mathrm{p}}}\right) + \left[s_{34}\right]\left(\sigma_{33}^{\boxed{\mathrm{II}}\Delta\boldsymbol{\varepsilon}^{\mathrm{p}}} + \sigma_{33}^{\boxed{\mathrm{II}}\Delta\mathbf{s}\Delta\boldsymbol{\varepsilon}^{\mathrm{p}}}\right) + \left[s_{45}\right]\left(\sigma_{31}^{\boxed{\mathrm{II}}\Delta\boldsymbol{\varepsilon}^{\mathrm{p}}} + \sigma_{31}^{\boxed{\mathrm{II}}\Delta\mathbf{s}\Delta\boldsymbol{\varepsilon}^{\mathrm{p}}}\right)\right) \end{cases}$$

Appendix D. Proof of $\left[\boldsymbol{\Omega}^{\mathbf{e}}\right]\otimes\mathbf{n} = -\left(\left[\boldsymbol{\varepsilon}^{\mathrm{e}}\right]\times\mathbf{n}\right)^{\mathrm{T}} - \left(\boldsymbol{\alpha}^{\mathrm{S}}\right)^{\mathrm{T}} + \frac{1}{2}\mathrm{tr}\left(\boldsymbol{\alpha}^{\mathrm{S}}\right)\mathbf{I}$

The starting point is the expression of the surface-dislocations density tensor $\boldsymbol{\alpha}^{\mathrm{S}}$ given for small displacements by Eq.(18). Decomposing the elastic distortion into its symmetric and skew-symmetric parts leads to

(D.1) $$\left[\boldsymbol{\omega}^{\mathrm{e}}\right]\times\mathbf{n} = -\left[\boldsymbol{\varepsilon}^{\mathrm{e}}\right]\times\mathbf{n} - \boldsymbol{\alpha}^{\mathrm{S}}$$

Knowing that $\omega_{ij}^e = -\grave{o}_{ijk}\Omega_k^e$ (cf Eq.(57)), we have in rectangular Cartesian coordinates

(D.2) $$-\grave{o}_{ljk}\grave{o}_{ijm}\left[\Omega_m^e\right]n_k = -\grave{o}_{ljk}\left[\varepsilon_{ij}^e\right]n_k - \alpha_{il}^S$$

(D.3) $$-\left(\delta_{il}\delta_{km} - \delta_{lm}\delta_{ik}\right)\left[\Omega_m^e\right]n_k = -\grave{o}_{ljk}\left[\varepsilon_{ij}^e\right]n_k - \alpha_{il}^S$$

(D.4) $$-\delta_{il}\left[\Omega_k^e\right]n_k + \left[\Omega_l^e\right]n_i = -\grave{o}_{ljk}\left[\varepsilon_{ij}^e\right]n_k - \alpha_{il}^S$$

The trace of the last equation is

(D.5) $$-2\left[\Omega_k^e\right]n_k = -\alpha_{kk}^S$$

Subsequently, it gives

(D.6) $$\left[\Omega_l^e\right]n_i = -\grave{o}_{ljk}\left[\varepsilon_{ij}^e\right]n_k - \alpha_{il}^S + \frac{1}{2}\alpha_{kk}^S\delta_{il}$$

which also writes

(D.7) $$\left(\left[\boldsymbol{\Omega}^{\mathbf{e}}\right]\otimes\mathbf{n}\right)^{\mathrm{T}} = -\left[\boldsymbol{\varepsilon}^{\mathrm{e}}\right]\times\mathbf{n} - \boldsymbol{\alpha}^{\mathrm{S}} + \frac{1}{2}\mathrm{tr}\left(\boldsymbol{\alpha}^{\mathrm{S}}\right)\mathbf{I}$$

Taking the transposed of this equation, we finally retrieve the expression of Eq.(64). To the authors' knowledge, this expression and the attached proof was not given in the literature.

References

Acharya, A., 2001. A model of crystal plasticity based on the theory of continuously distributed dislocations. J. Mech. Phys. Solids 49, 761-784.

Acharya, A., 2004. Constitutive analysis of finite deformation field dislocation mechanics. J. Mech. Phys. Solids 52, 301-316.

Acharya, A., Roy, A., 2006. Size effects and idealized dislocation microstructure at small scales: predictions of a phenomenological model of mesoscopic field dislocation mechanics: Part I. J. Mech. Phys. Sol. 54, 1687-1710.

Acharya, A., 2007. Jump condition for GND evolution as a constraint on slip transmission at grain boundaries. Phil. Mag. 87, 1349-1359.

Acharya, A., Beaudoin, A., Miller, R., 2008. New perspectives in plasticity theory: dislocation nucleation, waves, and partial continuity of plastic strain rate. Math. Mech. Sol. 13, 292-315.

Ashby, M.F., 1970. The deformation of plastically non-homogeneous materials. Philos. Mag. 21, 399-424.

Beausir, B., Fressengeas, C., Gurao, N.P., Töth, L.S., Suwas, S., 2009. Spatial correlation in grain misorientation distribution. Acta Mater. 57, 5382-5395.

Berbenni, S., Berveiller, M., Richeton, T., 2008. Intra-granular plastic slip heterogeneities: discrete vs. mean field approaches. Int. J. Solids Struct. 45, 4147–4172.

Berveiller, M., 1978. Contribution à l'étude du comportement plastique et des textures de déformation des polycristaux métalliques. Thesis, Université Paris-Nord, Villetaneuse.

Berveiller, M., Zaoui, A., 1980. Généralisation du problème de l'inclusion et application à quelques problèmes d'élastoplasticité des matériaux hétérogènes. J. Mécanique 19(2), 343-361.

Berveiller, M., Fassi-Fehri, O., Hihi, A., 1987. The problem of two plastic and heterogeneous inclusions in an anisotropic medium. Int. J. Eng. Sci. 25 (6), 691–709.

Bilby, B.A., 1955. In: Bristol Conference Report on Defects in Crystalline Solids, The Physical Society, London, 123.

Bullough, R., Bilby, B.A., 1956. Continuous distributions of dislocations: surface dislocations and the crystallography of Martensitic transformations. Proc. Phys. Soc. B 69, 1276-1286.

Christian, J.W., Crocker, A.G., Dislocations and lattice transformations, in: Dislocations in Solids (Vol. 3), F.R.N. Nabarro (ed.), Amsterdam, North Holland, 1980.

Franciosi, P., Berbenni, S., 2007. Heterogeneous crystal and polycrystal plasticity modeling from transformation field analysis within a regularized Schmid flow law. J. Mech. Phys. Solids 55, 2265–2299.

Franciosi, P., Berbenni, S., 2008. Multi-laminate plastic-strain organization for non-uniform TFA modeling of poly-crystal regularized plastic flow. Int. J. Plast. 24, 1549-1580.

Frank, F.C., 1950. In: Symposium on The Plastic Deformation of Crystalline Solids, Mellon Institute, Pittsburgh, (NAVEXOS-P-834), p.150.

Gemperlova, J., Paidar, V., Kroupa, F., 1989. Compatibility stresses in deformed bicrystals. Czech. J. Phys. B 39, 427-446.

Hadamard, J., 1903. Leçons sur la propagation des ondes et les équations de l'hydrodynamique, Paris:Herman.

Hirth, J.P., 1972. The influence of grain boundaries on mechanical properties. Metall. Transactions 3, 3047-3067.

Hirth, J.P., Lothe, J., 1982. Theory of dislocations. Wiley, New York.

Indenbom, V.L., 1966. Internal stresses in crystals. In: Theory of Crystal Defects, Academy of Sciences, Prague, pp. 257-274.

Kröner, E., 1958. Kontinuumstheorie der Versetzungen und Eigenspannungen. Springer-Verlag, Berlin.

Kröner, E., 1981. Continuum theory of defects in physics of defects. In: R. Balian et al., Editors, Les Houches, Session XXXV, North Holland Publishing Company.

Kröner, E., 1989. Modified Green functions in the theory of heterogeneous and/or anisotropic linearly elastic media. In: G.J. Weng, M. Taya, M. Abe (Eds.), Micromechanics and Inhomogeneity. Springer, Berlin, pp. 197–211.

Liang, H., Dunne, F.P.E., 2009. GND accumulation in bi-crystal deformation: Crystal plasticity analysis and comparison with experiments. Int. J. Mech. Sci. 51, 326-333.

Mach, J., 2009. PhD thesis, University of Illinois at Urbana Champaign.

Mach, J., Beaudoin, A.J., Acharya A., 2010. Continuity in the plastic strain rate and its influence on texture evolution. J. Mech. Phys. Solids 58, 105-128.

Mayama, T., Ohashi, T., Kondou, R., 2009. Geometrically necessary dislocation structure organization in FCC bicrystal subjected to cyclic plasticity. Int. J. Plast. 25, 2122-2140.

Michelitsch, T., Wunderlin, A., 1996. Stress functions and internal stresses in linear three-dimensional anisotropic elasticity. Z. Phys. B 100, 53-56.

Mura, T., 1963. Continuous distribution of moving dislocations. Philos. Mag. 89, 843-857.

Nye, J.F., 1953., Some geometrical relations in dislocated crystals. Acta Metall. 1, 153-162.

Ohashi, T., Barabash, R.I., Pang, J.W.L., Ice, G.E., Barabash, O.M., 2009. X-ray microdiffraction and strain gradient crystal plasticity studies of geometrically necessary dislocations near a Ni bicrystal grain boundary. Int. J. Plast. 25, 920-941.

Peirce, D., Asaro, R.J., Needleman, A., 1983. Material rate dpendence and localized deformation in crystalline solids. Acta Metall. 31, 1951-1976.

Peirce, D., Shih, C.F., Needleman, A., 1984. A tangent modulus method for rate dependent solids. Comput. Struct. 18, 875-887.

Puri, S., Das, A., Acharya, A., 2011. Mechanical response of multicrystalline thin films in mesoscale field dislocation mechanics. J. Mech. Phys. Solids 59, 2400-2417.

Qamar, I., Husain, S.W., 1989. Incompatibility stresses at the boundary of a bicrystal of an elastically anisotropic solid. Scipta Metall. 23, 2105-2110.

Rey, C., Saada, G., 1976. The elastic field of periodic dislocation networks. Philos. Mag. 33 (5), 825–841.

Rey, C., Zaoui A., 1980. Slip heterogeneities in deformed aluminium bicrystals. Acta Metall. 28, 687-697.

Rey, C., Zaoui A., 1982. Grain boundary effects in deformed bicrystals. Acta Metall. 30, 523-535.

Richeton, T., Wang, G.F., Fressengeas, C., 2011. Continuity constraints at interfaces and their consequences on the work hardening of metal-matrix composites. J. Mech. Phys. Solids 59, 2023-2043.

Saada, G., 1979. Elastic field of dislocation networks and grain boundaries. Acta Metall. 27, 921–931.

Saada, G., 2006. Planar dislocation arrays and crystal plasticity. In: Buschow, K.H.J. et al. (Eds.), Encyclopedia of Materials: Science and Technology. Elsevier, pp. 1–18.

Schick, A., Fritzen, C.P., Floer, W. Hu, Y.M., Krupp, U., Christ, H.J., 2000. Stress concentrations at grain boundaries due to anisotropic elastic material behavior. Struct. Mater. 6, 393-402.

Stupkiewicz, S., Petryk, H., 2002. Modelling of laminated microstructures in stress-induced martensitic transformations. J. Mech. Phys. Solids 50, 2303-2331.

Suezawa, M., Sumino, K., 1976. Behaviour of elastic constants in Cu-14wt.% Al-4.2wt.% Ni alloy in the close vicinity of Ms-point. Scipta Metall. 10, 789-792.

Sun, S., Adams, B.L., Shet, C., Saigal, S., King, W., 1998. Mesoscale investigation of the deformation field of an aluminium bicrystal. Scripta Mater. 39, 501-508.

Sutton, A.P., Balluffi, R.W., 1995. Interfaces in Crystalline Solids, Oxford University Press.

Taupin, V., Berbenni, S., Fressengeas, C., 2012. Size effects on the hardening of channel-type microstructures: a Field Dislocation Mechanics-based approach. Acta Mater. 60, 664-673.

Takeuchi, T., 1975. Work hardening of copper single crystals with multiple glide orientations. Trans. JIM 16, 629-640.

Tewary, V.K., Wagoner, R.H., Hirth, J.P., 1989. Elastic Green's function for a composite solid with a planar interface. J. Mater. Res. 4, 113-123.

Vehoff, H., Laird, C., Duquette, D.J., 1987. The effect of hydrogen and segregation on fatigue crack nucleation at defined grain boundaries in nickel bicrystals. Acta Metall. 35, 2877-2886.

Vehoff, H., Nykyforchyn, A., Metz, R., 2004. Fatigue crack nucleation at interfaces. Mat. Sci. Eng. A 387-389, 546-551.

Willis, J.R., 1967. Second order effects of dislocations in anisotropic crystals. Int. J. Eng. Sci. 5, 171-190.

Yaguchi, H., Margolin, H., 1986. Grain boundary contribution to the Bauschinger effect in Beta-Brass bicrystals. Metall. Transactions A 17A, 2017-2029.

Figures captions

	Cubic stiffnesses	*Isotropic stiffnesses (Voigt average)*
Cu	c_{11} = 170 GPa c_{12} = 124 GPa c_{44} = 75 GPa	E = 144 GPa ν = 0.33
Al	c_{11} = 107 GPa c_{12} = 61 GPa c_{44} = 28 GPa	E = 70 GPa ν = 0.35

Table 1. Values of elastic stiffnesses for Cu and Al.

n = 20 V_0 = 10^{-11} m.s^{-1} ρ_m = 1.10^8 m^{-2} σ_h = 4.2 MPa	**Orientation of Crystal I** Crystal directions: $[123]$; $[5\bar{4}1]$ Global directions: $[010]$; $[101]$
	Orientation of Crystal II Crystal directions: $[223]$; $[33\bar{4}]$ Global directions: $[010]$; $[100]$

Table 2. Material parameters used in the FE simulation.

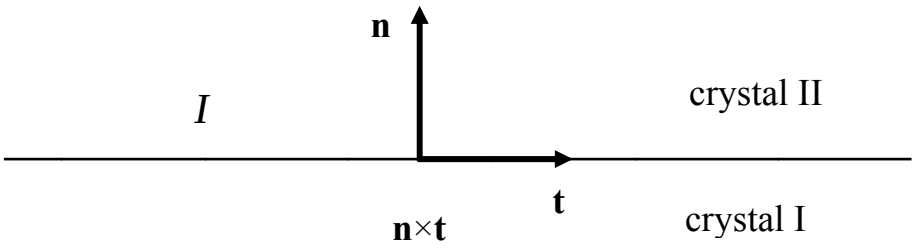

Figure 1. Sketch of interface *I* between crystals I and II, with unit normal vector **n**. The unit vector **t** is an arbitrary vector in the interface.

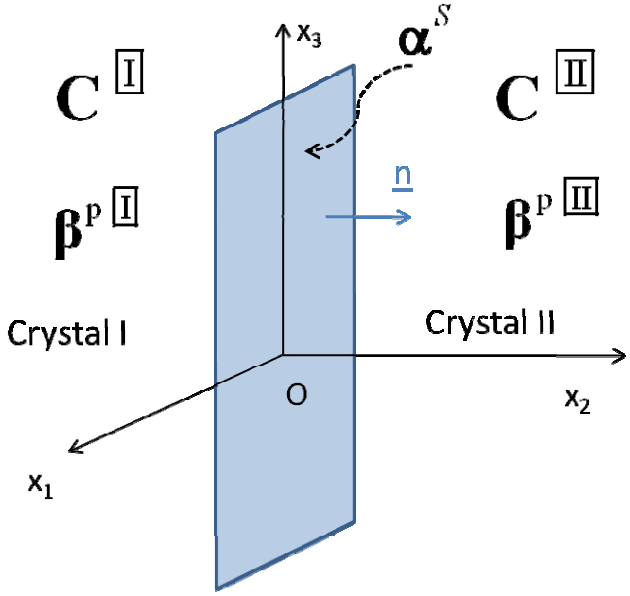

Figure 2. Configuration describing an infinite planar grain boundary characterized by an interface dislocation density tensor $\boldsymbol{\alpha}^S$.

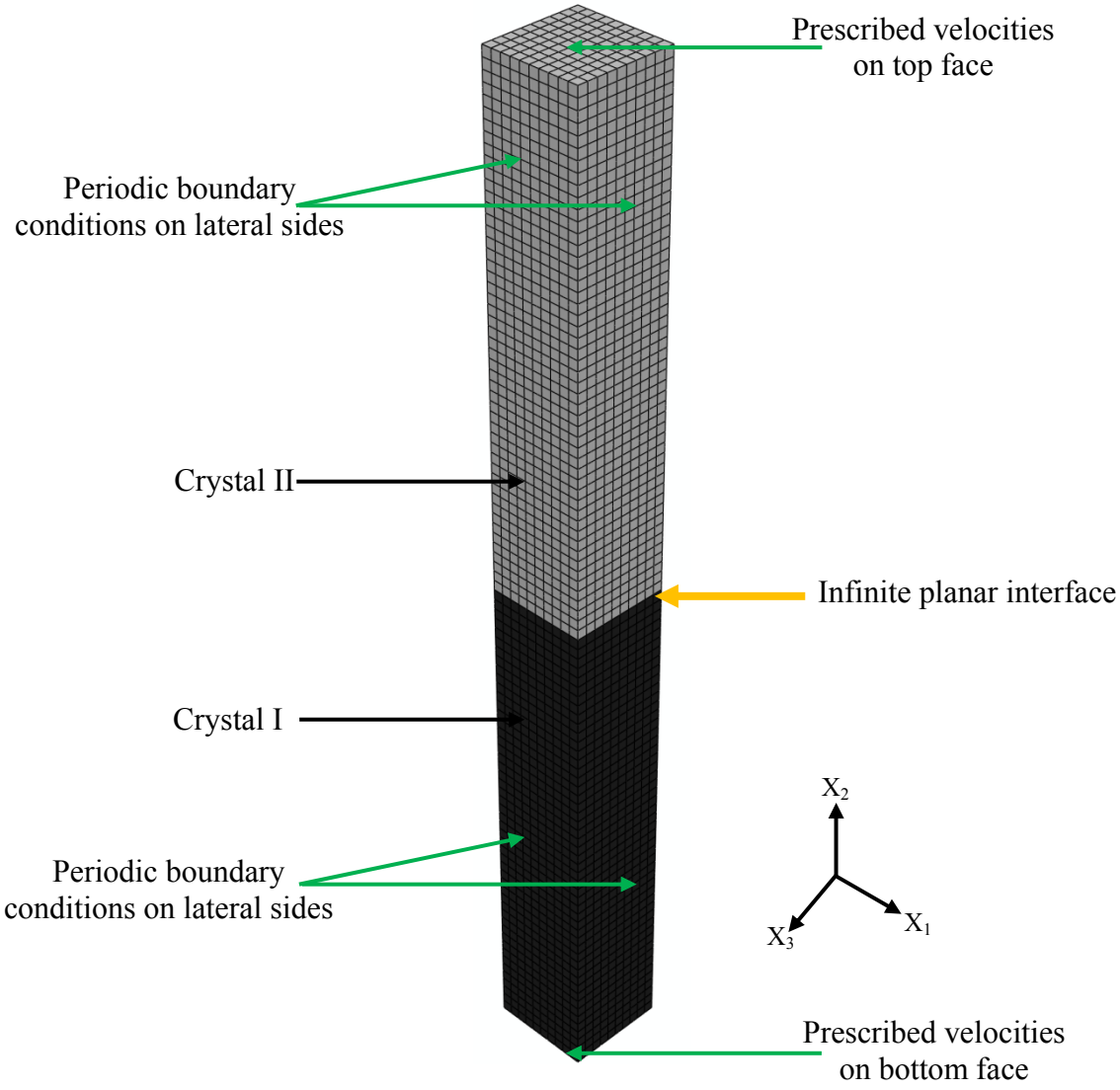

Figure 3. Sketch of the bicrystal bar used in the FE simulation.

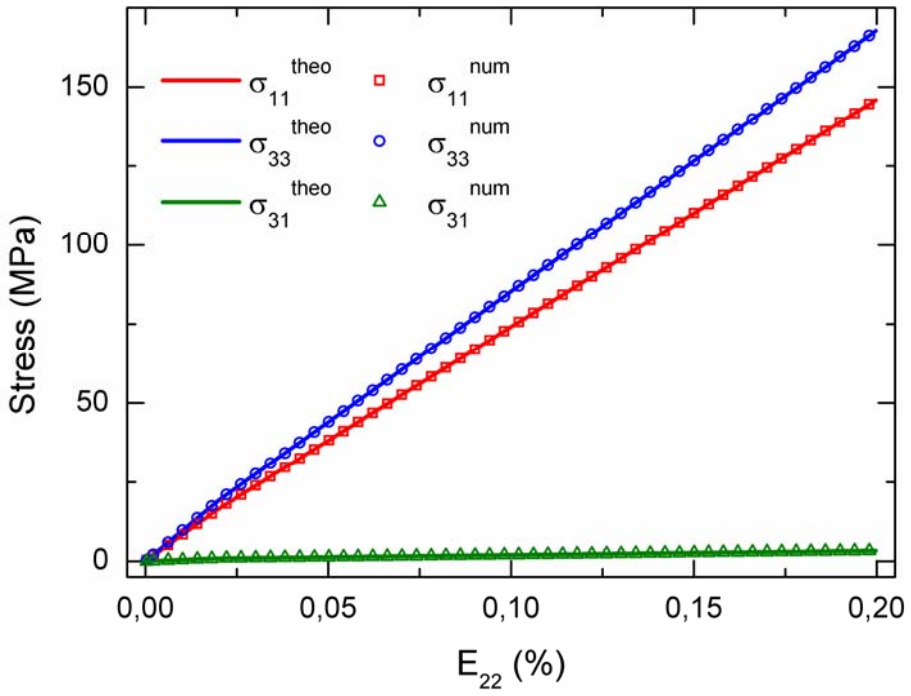

Figure 4. Comparison between the stresses in crystal II provided by the FE simulation (σ_{ij}^{num}) and those directly derived from the analytical formulas (σ_{ij}^{theo}).

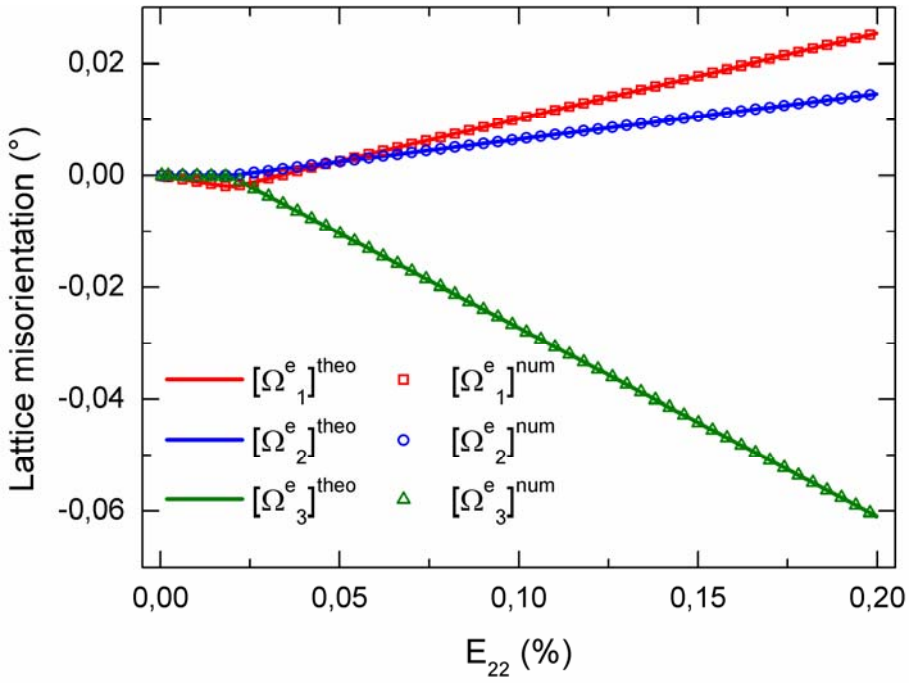

Figure 5. Comparison between the lattice misorientations provided by the FE simulation ($\left[\boldsymbol{\Omega}_i^{\mathrm{e}}\right]^{num}$) and those directly derived from the analytical formulas ($\left[\boldsymbol{\Omega}_i^{\mathrm{e}}\right]^{theo}$).

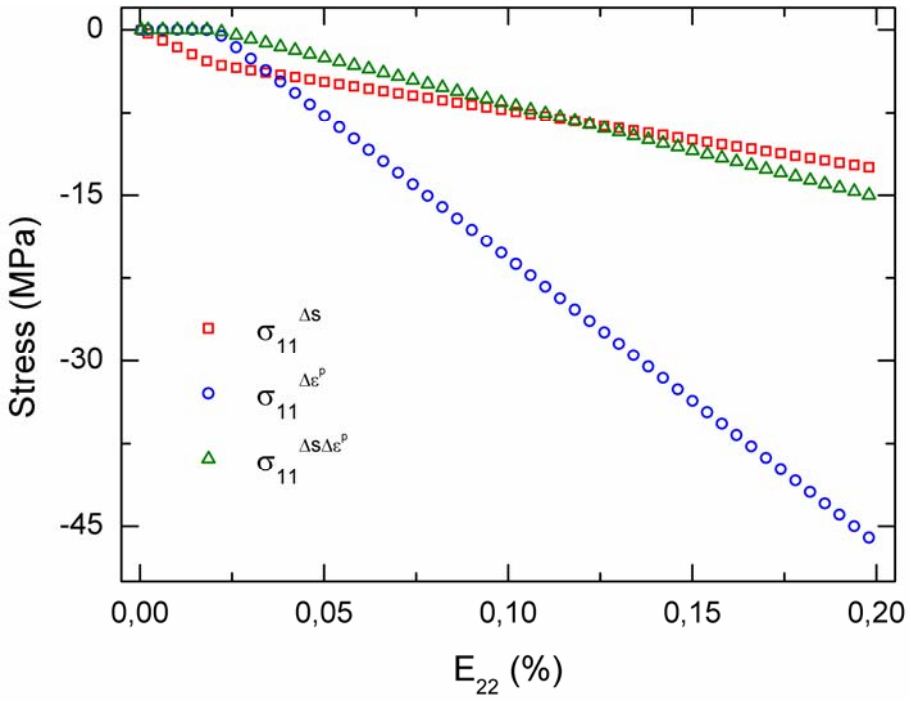

Figure 6. Contribution of the different incompatibility source terms for σ_{11} in crystal II (cf. Eq.(46)).

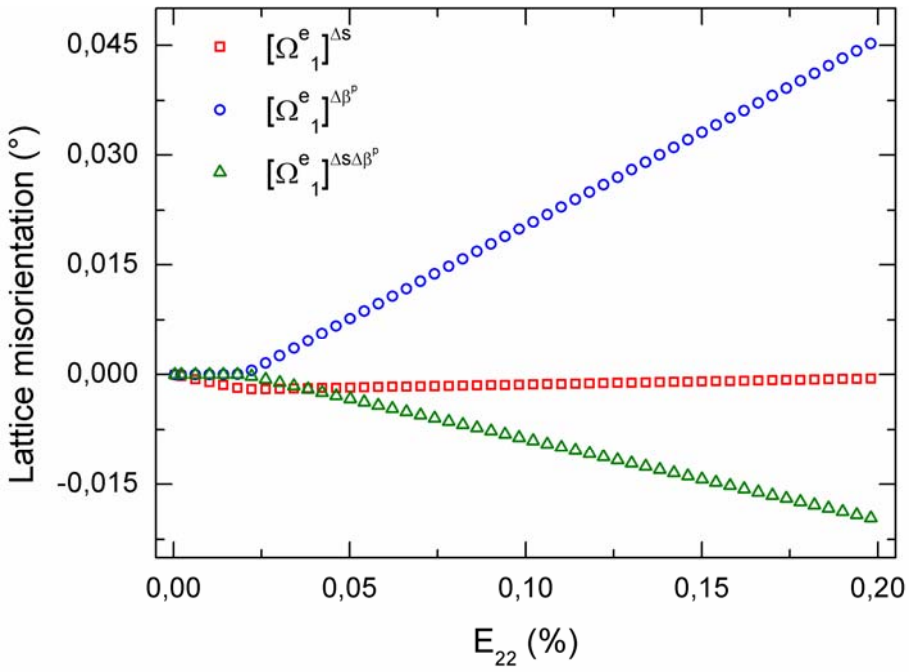

Figure 7. Contribution of the different incompatibility source terms for $\left[\Omega_1^e\right]$ (cf. Eq.(62)).

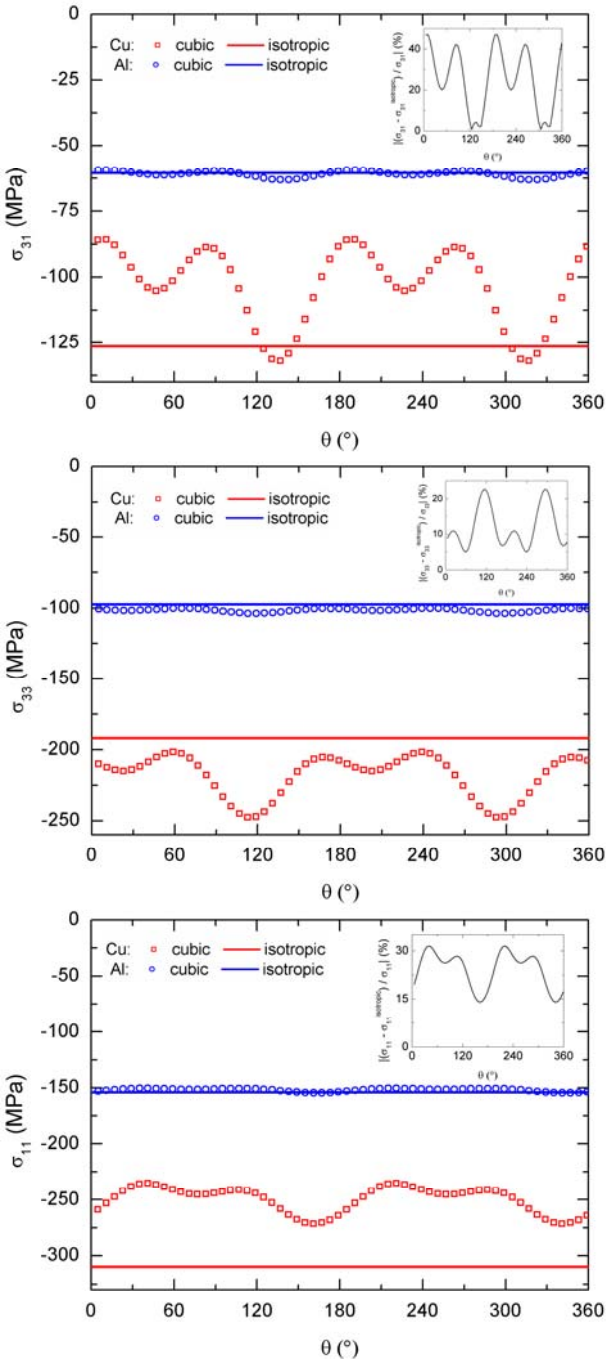

Figure 8. Evolution of the residual stress components σ_{11}, σ_{33}, σ_{31} in crystal II with the angle θ for $\gamma = 0.01$. Crystal I remains fixed while crystal II can rotate around (O,x_2) by the angle θ. Inset: relative error made by the isotropic approximation for Cu.

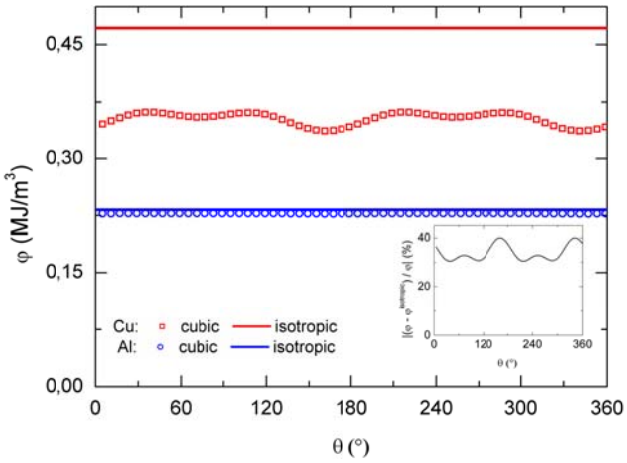

Figure 9. Evolution of the stored elastic energy density φ in crystal II with the angle θ for $\gamma = 0.01$. Crystal I remains fixed while crystal II can rotate around (O,x_2) by the angle θ. Inset: relative error made by the isotropic approximation for Cu.

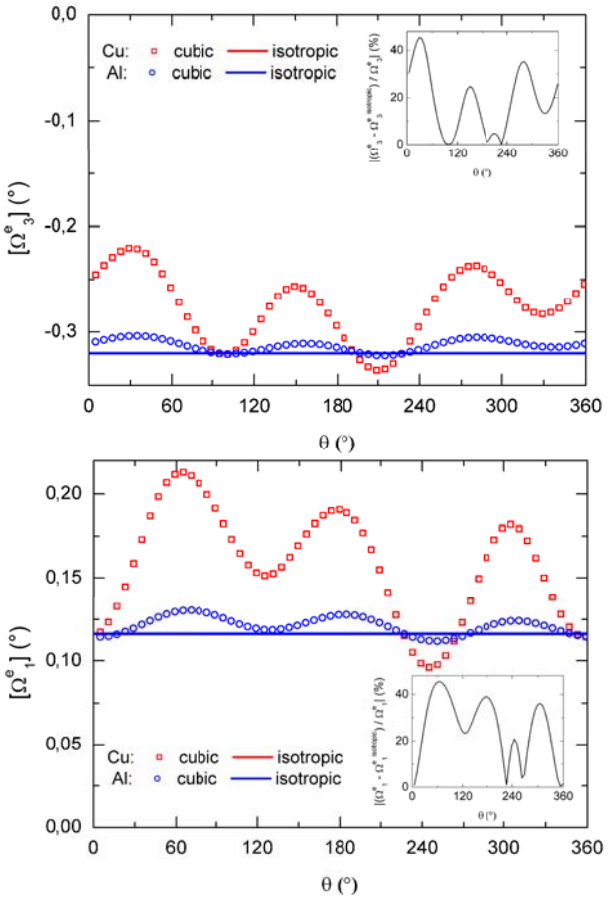

Figure 10. Evolution of the residual lattice misorientation vector components $\left[\Omega_1^e\right]$ and $\left[\Omega_3^e\right]$ in crystal II with the angle θ for $\gamma = 0.01$. Crystal I remains fixed while crystal II can rotate around (O,x_2) by the angle θ. Inset: relative error made by the isotropic approximation for Cu.